Mass Transfer of Oxygen across the Capillary Fringe

Dissertation

zur Erlangung des Grades eines Doktors der Naturwissenschaften

der Geowissenschaftlichen Fakultät
der Eberhard Karls Universität Tübingen

vorgelegt von
Sanheng Liu
aus China

2008

Tag der mündlichen Prüfung: 30, 05, 2008

Dekan: Prof. Dr. Peter Grathwohl

1. Berichterstatter: Prof. Dr. Peter Grathwohl

2. Berichterstatter: Prof. Dr. Ulrich Mayer

Abstract

Mass transfer of oxygen from soil air across the capillary fringe affects the fates of many contaminants in groundwater. The processes involved in mass transfer include aqueous and gas phase molecular diffusion, mechanical dispersion, reaction and partitioning between the aqueous and gas phases. The extent to which each of these processes contributes to mass transfer between the saturated and unsaturated zone depends on both the properties of the solute and the conditions within the subsurface. It is generally believed that transversal mixing controls the flux of electron acceptors such as oxygen across the capillary fringe into groundwater.

The objective of this work is to investigate the transfer of oxygen between soil gas and groundwater. The thesis consists of three parts: the numerical simulations, derivation of analytical solutions, and high resolution data bench scale tank experiments for the validation of the models.

Numerical simulation results show that in both reactive and non-reactive cases the oxygen gradient increases rapidly when the water saturation reaches about 85%. The maximum product concentration does not depend on the concentration of oxygen. Instead, it increases proportionally to the concentration of electron donor. Results from the numerical simulation also show that due to a lower horizontal flow velocity in the not fully saturated capillary fringe, the reaction product accumulates there. New analytical solutions were derived in order to predict the spatial distribution of the reactants and the reaction product as well as the length of electron donor plumes.

The tank experiments show that only a minor oxygen gradient develops in the unsaturated zone. Steep concentration gradients develop in the saturated capillary fringe, which indicates that mass transfer becomes dispersion dominated. For a flow velocity of 7.33 m/day, the contribution of diffusion to the overall mass transfer coefficient is only 10%. The dispersion coefficients obtained for the reactive and non-reactive cases are the same.

Kurzfassung

Der Transport von Sauerstoff aus der Bodenluft über den Kapillarsaum beeinflusst den Abbau vieler Schadstoffe und sonstiger Stoffumsätze im Grundwasser. Dabei schließen die am Stofftransport beteiligten Prozesse die molekulare Diffusion in der wässrigen sowie der gasförmigen Phase, die mechanische Dispersion sowie die Reaktion und Verteilung zwischen wässriger und gasförmiger Phase mit ein. Das Ausmaß, mit welchem jeder dieser Prozesse zum Stofftransport zwischen gesättigter und ungesättigter Zone beiträgt, hängt sowohl von den Eigenschaften der gelösten Stoffe wie auch von den Bedingungen im Untergrund ab. Es wird allgemein angenommen, dass die transversale Dispersion den Fluss von Elektronenakzeptoren, wie beispielsweise Sauerstoff, über den Kapillarsaum ins Grundwasser kontrolliert.

Gegenstand dieser Arbeit ist die detaillierte Untersuchung des Übergangs von Sauerstoff aus der Bodenluft ins Grundwasser und die Quantifizierung der limitierenden Parameter. Die Doktorarbeit setzt sich aus drei Teilen zusammen, wobei der erste Teil die numerischen Simulationen umfasst; der zweite Teil beschäftigt sich mit der Ableitung analytischer Lösungen, um abschließend auf die im Labormaßstab durchgeführten Tankexperimente einzugehen, mit denen hoch aufgelöste Datenreihen für die Validierung der numerischen Modelle gewonnen werden konnten.

Die Ergebnisse der numerischen Simulationen zeigen, dass der Sauerstoffgradient sowohl im reaktiven wie im nicht-reaktiven Fall schnell größer wird, sobald die Wassersättigung einen Wert von etwa 85 % erreicht. Die maximale Konzentration des Reaktionsprodukts ist nicht von der Sauerstoffkonzentration abhängig, sondern nimmt stattdessen proportional zur Konzentration des Elektronendonators zu. Ebenso zeigen die Ergebnisse der numerischen Simulation, dass es aufgrund der kleineren horizontalen Fließgeschwindigkeiten im nicht voll gesättigten Bereich des Kapillarsaums zur Akkumulation des Reaktionsprodukts in dieser Zone kommt. Zusätzlich wurden neue, vereinfachte analytische Lösungen hergeleitet, um die räumliche Verteilung der Edukte und des Produkts sowie die Länge der Elektronendonator-Fahnen vorherzusagen.

Die Tankexperimente zeigen, dass sich in der ungesättigten Zone nur ein flacher O_2-Konzentrationsgradient einstellt. Im gesättigten Kapillarsaum kommt es dagegen zu steilen Konzentrationsgradienten, was belegt, dass der Stofftransport durch Dispersion im Wasser dominiert wird. Für eine Fließgeschwindigkeit von 7,33 m/d beträgt der Anteil der Diffusion am Stoffübergangskoeffizienten nur 10 %. Die Dispersionskoeffizienten, welche für den reaktiven und nicht-reaktiven Fall mit hoher Genauigkeit experimentell ermittelt wurden, sind nicht signifikant verschieden, wie durch die Theorie vorhergesagt.

ACKNOWLEDGEMENTS

I would like to thank my advisor Prof. Dr. Peter Grathwohl for providing me the chance to do this research in his group, for his suggestions and encouragements which helped me out whenever I was entrapped in capillary fringe.

A big thanks to Prof. Dr. Ulrich Mayer, for not only helping me with the numerical modeling with MIN3P but also evaluating my thesis. The numerical modeling work would also have not been done without Dr. Uli Maier who helped me get started and implemented the code with compound specific diffusion. For the analytical part of my thesis I want to thank Prof. Dr. Rudolf Liedl for his good suggestions and comments.

I want to thank our tank artist Christina Eberhardt for her help with the setup of tank experiments and discussions which saved me a lot of time. For the measurement of sulfite and sulfate with Ion Chromatography I want to thank Annegret Walz and Thomas Wendel. Thomas helped me find a method to stabilize sulfite. For his good suggestions regarding the non-invasive measurement of oxygen I want to thank Robert Bauer. For the build up of the tank I want to thank our technician Wolfgang Kürner for his skillful work. Dr. Matthias Piepenbrink deserves my special thanks for the help in the beginning of my thesis.

I also want to thank all my colleagues for such a nice working group, especially those who had been working with me in the big office (U5-U7), including Christina, Dietmar, Ilka, David, Alicia, Andrea, Kerstin und Marina. Ich werde den Stocherkahn, internationals Abendessen, den Filmabend und Würfel &Karten Spiele vermissen. I am very grateful to the various helps from Christina Haberer.

Thank you Guohui, Danyang, Jie and Lihua for the ‘Chinese corner’ and Chinese food.

Finally I want to thank my family for being there for me all the time.

Contents

List of Abbreviations

C_{A0}: Oxygen concentration at the upper boundary of the capillary fringe [mol. l^{-1}]
C_{bg}: Background oxygen concentration [mol. l^{-1}]
C_{B0}: Initial concentration of electon donor [mol. l^{-1}]
C_{max}: Maximum concentration of reaction product [mol.l^{-1}]
C_{norm}: Normalized oxygen concentration [-]
D_{air} : Diffusion coefficient in air [$m^2.s^{-1}$]
D_{aq}: Aqueous phase diffusion coefficient [$m^2.s^{-1}$]
D_e : Effective diffusion coefficient [$m^2.s^{-1}$]
D_{tA} : Hydrodynamic dispersion coefficients of oxygen [$m^2.s^{-1}$]
D_{tB} : Hydrodynamic dispersion coefficients of electron donor [$m^2.s^{-1}$]
D_z : Hydrodynamic transversal dispersion coefficient [$m^2.s^{-1}$]
D_{pore} : Pore diffusion coefficient [$m^2.s^{-1}$]
$F(x)$: Oxygen flux at location x [mol.m.s^{-1}]
F_{total}: Total oxygen flux into the system [mol.$m^2.s^{-1}$]
h_1: Hydraulic head at the inlet [m]
h_2 : Hydraulic head at the outlet [m]
h_{inital} : Initial water table in the tank [m]
H: Henry's law constant [l.atm.mol^{-1}]
K: Hydraulic conductivity [m.s^{-1}]
K_s : Hydraulic conductivity at water saturation [m.s^{-1}]
l: van Genuchten parameter [-]
L: The length of the tank [m]
m: van Genuchten parameter [-]
M : Thickness of the aquifer [m]
n: porosity [-]
P_A : Oxygen partial pressure
Pe: Peclet number [-]
q: Darcy's flux [m.s^{-1}]
Q: Pumping rate [$m^3.s^{-1}$]
v : Pore velocity [m.s^{-1}]
Y_1: Stoichiometry of oxygen [-]
Y_2 : Stoichiometry of electron donor [-]
α: van Genuchten parameter [m^{-1}]
α_l : Longitudinal dispersivity [m]
α_t : Transverse dispersivity [m]
θ : Volumetric water saturation [-]
θ_r : Residual saturation [-]
θ_s : equals to 1.
γ : Reaction product formation rate [mol.$l^{-1}.s^{-1}$]

1. Introduction

1.1 Motivation

Transport of oxygen from the unsaturated zone to groundwater plays an important role in many subsurface processes, especially for the natural attenuation of hydrocarbons and related organic contaminants or ammonia contaminated aquifers, where oxygen supply is a controlling factor. Most of these compounds are rapidly degradable in the presence of oxygen. However, exchange of oxygen with subsurface contaminant plumes is often slow. In many aquifers, oxygen, which is the primary electron acceptor in microbial hydrocarbon degradation, is absent or present in low concentrations. Understanding O_2 transfer also assists our understanding of the exchange of other gases between the unsaturated zone and groundwater, e.g., the greenhouse gases CH_4 and N_2O, which have been studied by soil scientists and climatologists, and also some atmospheric trace gases like chlorofluorocarbons and SF_6, which are of great interest to hydrologists.

1.2 Objectives

The overall objectives of this study were to better understand mass transfer of oxygen between the unsaturated and saturated zone and to investigate the influence of groundwater flow velocities and the reaction on the magnitude of transverse dispersion in porous media.

The first task was to find out the oxygen spatial distribution through a numerical model and simplified mathematical model for the reactive and conservative cases.

The second task was to carry out well-controlled bench scale tank experiments. These experiments were to verify the models and to obtain the hydrodynamic dispersion coefficients for the reactive and conservative cases under different velocities.

1.3 Thesis outline

Chapter 2 consists of a literature review of the previous work, in particular the most important findings regarding mass transfer in the capillary fringe of aquifers.

Chapter 3 provides the theory of capillarity and horizontal flow of water in the capillary fringe. This determines the boundary conditions of the numerical and analytical models (Chapter 4).

Chapter 4 gives a mathematical deduction of the oxygen penetration depth, reactants distribution, and oxygen fluxes in the soil, as well as the length of a reactive contaminant plume. The supplemented numerical modelling is used to verify some of the simplifications needed in the analytical solution. An accumulation of reaction product in the unsaturated zone is predicted by the numerical model and the analytical solution.

Chapter 5 validates the analytical solutions from Chapter 4 with high resolution experimental data from bench scale tank experiments and provides a new method to determine hydrodynamic dispersion coefficients using oxygen as a non- reactive and reactive tracer.

Chapter 6 is a summary of the previous chapters, which addresses the research objectives in chapter 1.

2. Literature review

2.1 Saturation and matrix potential

A number of definitions of the capillary fringe exist within the literature. All of these definitions accept the water table (p = gauge pressure = 0) as the lower limit on the CF. Differences among the definitions are generally related to the definition of the upper limit of the CF (Berkowitz et al., 2004). In field conditions drying and wetting processes driven by water table changes may cause the thickness and location of the capillary fringe to change with time. While the influence of the gravitational potential on the amount of water is identical for drying and wetting processes, the relation between matric potential and water content may depend on wetting and drying history. For a given matric potential the water content may vary within wide limits. In various extensions of the capillary fringe, the water content, pore water velocity, and hydraulic conductivity change according to saturation. These variations modify the water, solute, and gas transport from the soil surface to the aquifer (Russo et al., 1989) and also the transport of volatile compounds from the aquifer to soil gas.
The soil water content and matric potential curve can be described by several models, for example, the van Genuchten model (van Genuchten, 1980) or Brooks Corey model (Brooks and Corey, 1964). The van Genuchten model assumes a gradual change of water content away from the table into the unsaturated part until a residual saturation is reached. The parameters that define the shape of van Genuchten curve can be obtained from some empirical relationships (Schaap et al., 1998) which are based on the soil textures. In contrast to the van Genuchten model, the Brooks & Corey model assumes that the water can still be fully saturated some distance above the water table as long as the matric potential is higher than a critical potential, i.e. the so-called air entry pressure which is directly related to the largest pore size through Young Laplace equation which describes the relationship between the capillary pressure and the radius of a tube. Such a fully saturated zone exists for very fine and homogeneous soil (Ronen et al., 1997).

Due to the introduction of this air entry pressure the water retention curve is not continuously differentiable, which complicates the numerical solution of Richard's equation. This is the reason why the van Genuchten model is more favourable in most

numerical codes. However, a water retention curve obtained from experiments is more appropriate. The matric potential can be measured with the tensiometer. For the measurement of water content, the three commonly used methods are neutron probe, gamma attenuation, and Time Domain Reflectometry (TDR). The hydraulic conductivity can be measured with double-ring infiltrometer.
This effect of a non-unique water-retention curve, the soil water hysteresis, is relevant for the gas-phase continuity within or near the capillary fringe (Lehman et al., 1998). However, after several wetting-drainage cycles, the hysteresis effect becomes less significant. Typically, the migration of multiple fluids in the subsurface is modelled as if it were independent of aqueous phase composition. However, solution conditions including pH, concentration of surface-active solutes, and ionic strength may impact the interfacial tension and the wettability of a system, which can be directly reflected in the capillary pressure-saturation relationship (Lord, et al., 1997a, 1997b) and this in turn may markedly affect subsurface transport.

2.2 Gas transport across the capillary fringe.

The transport of carbon dioxide in the unsaturated zone across the capillary fringe in sand (Caron et al., 1994) and to the moving groundwater (Caron et al., 1998) shows that the mass transfer rate of carbon dioxide across the capillary fringe is significantly slower than for an open surface and the capillary fringe offers a significant resistance to mass transfer. Similarly, the risk of groundwater contamination by volatile organic compounds like TCE has been studied (Klenk and Grathwohl, 2002; Jellali et al. 2003; McCarthy and Johnson, 1993). McCarthy and Johnson (1993) discussed the transport of volatile organic compounds across the capillary fringe and concluded that a one-dimensional approximation of the vertical transport across the capillary fringe can be used, with the dominant vertical transport mechanism being molecular diffusion. Another important finding from theses studies was that transverse vertical dispersion is essential for transfer of solutes across the capillary fringe. The dispersion coefficients observed, however, are significantly larger than in fully saturated porous media (Klenk and Grathwohl, 2002; Olsson and Grathwohl, 2007), indicating that the flow pattern in the capillary fringe is more complex than in the saturated zone and transient conditions enhance dispersion in the capillary fringe. Additionally, the salinity and capillary pressure (Lassin et al., 2005) and pH (Caron et al., 1994, 1998)

at the capillary fringe affect the thermodynamic and electrostatic properties of the capillary water, which will further affect the transport process especially in the reactive case.

2.3 Reactions in the capillary fringe.

Concerning reactions in the CF only a limited number of quantitative experimental studies are available. Many field studies only present speculations to explain certain observations (Ronen et al., 2000).

Due to the relative thinness of the capillary fringe ‘‘the hydrologist often neglects the capillary fringe’’ (Bear, 1979; p. 74). However, the height of the CF is a significant fraction of the interface region where most of the biological and chemical reactions occur. For the study of the chemical properties of groundwater, the neglect of the CF lacks adequate foundation since all contaminant fluxes arriving from the soil surface to bulk groundwater must flow, either vertically or horizontally, through this chemically reactive zone (Ronen et al., 2000). Ostendorf et al. (1995) suggested that microbiological activity near the CF had the effect of reducing the O_2 demand of a deicing agent (calcium magnesium acetate) on groundwater. Zaidelman et al. (1997) reported that maximum biochemical decomposition of organic matter within peaty soils treated with a cover farming system was observed within the CF. In one of the most comprehensive studies Lahvis et al. (1999) investigated the aerobic biodegradation and volatilization rates of gasoline hydrocarbons near the water table by extrapolating gas transport rates through the capillary zone. The results of this study indicate that aerobic biodegradation and volatilization of gasoline hydrocarbons within the CF can be an important pathway to the natural attenuation of hydrocarbons at gasoline spill sites.

Substantial quantities of gas bubbles present in the immediate vicinity of the water table, indicating geochemical and/or microbial activity, have also been reported (e.g. Ronen et al., 1989). Microbial respiration rates through a 3.2-m-thick ‘mesocosm’ was measured (Hendry et al., 2001) and the result shows a non-negligible respiration rate in the CF, which increased upwards into the partially saturated zone.

2.4 LNAPL in the capillary fringe.

A number of studies exist concerning the behavior of light non-aqueous phase liquids (LNAPL) in the CF, which can be seen as an analogous to the two phases system air (non-wetting fluid) and water (wetting fluid). Jawitz et al. (1998) investigated variations in the structure of the CF with respect to the distribution and displacement of the LNAPL in the CF. They show how LNAPLs entrapment is caused by rising water tables that create problems with the removal of pollutants from the aquifer. Circumstantial field evidence suggests that heterogeneous flow and transport processes in the CF are likely to form local traps for LNAPLs in the liquid phase and dense volatiles in the gas phase (Ronen et al., 1997). The relatively small spill volume which is trapped by the capillary forces in the unsaturated zone might represent a long-lasting source of contamination to the air, soil and groundwater due to volatilization, dissolution, and partitioning of its compounds (Thibodeaux, 1979; Baehr, 1987; Jury et al., 1990). Hu et al. (2006) reported that LNAPLs spread from a leaking pipe downwards due to gravity forces, forming a high concentration zone above the capillary fringe and then spreading out laterally along the groundwater table.

2.5 Mixing and diffusion phenomena in the capillary fringe.

Lehman et al. (1998) argued that variations in water content and matrix potential in the CF region caused by the fluctuating water table influence aeration and hence various chemical and microbial processes. It was also demonstrated in laboratory experiments that fluctuating the water table enhanced the degradation of diesel oil (Rainwater et al., 1993). Similarly, in laboratory experiments and in wastewater treatment plants, it was demonstrated that an alternating regime of aerobic-anaerobic conditions stimulated the complete mineralization of various contaminants including chlorinated compounds (Zitomer and Speece, 1993). The dynamic regime imposed by a fluctuating water table and the resulting differences in soil aeration, not only affect the microbial and chemical reactions that organic pollutants undergo but also the transport of gases and solutes through the aquifer (Sinke et al., 1998). Affek et al. (1998) suggested that high CO2 concentrations in the CF may indicate a decrease in the diffusivity of the CF relative to the unsaturated zone. Direct field measurements have demonstrated that the high moisture content sustained in the CF can aid movement of pesticides along preferential pathways (Haria et al., 2003), how the CF

can act to concentrate Cr and result in contamination of groundwater (Khan and Puls, 2002), and how salt can become concentrated in the CF region due to irrigation and upward water flux from the water table (Slavich et al., 2002). Silliman et al. (2002) demonstrated that heterogeneity can lead to fluid movement, distinct from the effects of the boundaries, from below the water table into the CF. Dunn and Silliman (2003) demonstrated the presence of entrapped air in the region bounding the water table due to the air entry barriers (AEBs) or the inability of this coarse zone to drain until the pressure in the overlying fine sand is below the air-entry barrier for the fine sand. Berkowitz et al. (2004) suggested that this transition zone be referred to as the partially saturated fringe (PSF) adjacent to the water table. The partially saturated capillary fringe is limited from above by the lower portion of the unsaturated zone, where fluid movement is dominated by gravity-driven flow and fingering, and from below by the upper portion of the groundwater zone, characterised by fully three dimensional flows and a discontinuous air phase. The lower boundary is not considered to the water table but somewhere below the water table as has been shown in this paper. They also suggested that currently an adequate definition describing the behaviour of the CF at local scale does not exist. The experimental and modelling results from Berkowitz et al. (2004) also indicate that vertical and horizontal flux within the CF can dramatically alter fluxes at the local scale, and potentially, influence chemical transport, geochemistry, and microbial dynamics.

2.6 Microorganisms in the capillary fringe.

The coexistence of large quantities of water and air within the capillary fringe makes the CF a suitable environment for biodegradation processes as well as other important chemical reactions (Affek et al., 1998; Sinke et al., 1998). Biosurfactants generated through microbial colonization can reduce the air-liquid surface tension or modify the solid-liquid contact angle (Neu, 1996; Rockhold et al., 2004). Microbial colonization causes localized drying within the colonized zone, with decreases in saturation approaching 50% of antecedent values, and a 25% lowering of the capillary fringe height (Yarwood et al., 2006). Brown and Jaffe (2006) showed that nonionic surfactants change wetting angles and thus the behaviour of microorganisms.

Additionally, a series of laboratory experiments has demonstrated the ease with which bacteria can be transported from the groundwater zone into the CF by advective motion of the pore water. The migration of the bacteria was also observed to be substantially influenced by the presence of a trapped air phase below the water table and a coarse sand lens above the water table that remained at high moisture content due to the effect of air-entry barriers (Dunn et al., 2005).

References

Affek, H.P., Ronen, D., Yakir, D., 1998. About production of CO2 in the capillary fringe of a deep phreatic aquifer. Water Resour. Res. 34, 989–996.

Baehr, A.L., 1987. Selective transport of hydrocarbons in the unsaturated zone due to aqueous vapor phase partitioning. Water Resour. Res. 23, 1926-1938.

Berkovitz, B., Silliman, S.E., Dunn, A.M., 2004. Impact of the Capillary Fringe on Local Flow, Chemical Migration, and Microbiology. Vadose Zone Journal. 3, 534-548.

Brooks, R.H., Corey, A.T., 1964. Hydraulic properties of porous media. Hydrology Papers, Colorado State Univeristy, Ft. Collins.

Brown, J., Jaffe, M., 2006. Effects of nonionic surfactants on the cell surface hydrophobicity and apparent Hamaker Constant of Sphingomonas sp. ES&T 40, 195.

Caron, F., Manni, G., Workman, W.J.G., 1998. A large-scale laboratory experiment to determine the mass transfer of CO2 from a sandy soil to moving groundwater. J. Geochem. Explor. 64,111–125.

Caron, F., Wilkinson, S.R., Torok, J., Haas, M.K., Selander, W.N., 1994. CO2 transport through the capillary fringe in sand. Waste Manag. 14, 421-433.

Dunn, A.M., Silliman, S.E., 2003. Air and water entrapment in the vicinity of the water table: A laboratory study on heterogeneous sands. Ground Water. 41, 729–734.

Dunn, A.M., Silliman, S.E., Dhamwichukorn, S., Kulpa, C.F., 2005. Demonstration of microbial transport into the capillary fringe via advection from below the water table. Journal of Hydrology. 306(1-4), 50-58.

Haria, A.H., Hodnett, M.G., Johnson, A.C., 2003. Mechanisms of groundwater recharge and pesticide penetration to a chalk aquifer in southern England. J. Hydrol. 275,122–137.

Hendry, M.J., Mendoza, C.A., Kirkland, R., Lawrence, J.R., 2001. An assessment of a mesocosm approach to the study of microbial respiration in a sandy unsaturated zone. Ground Water. 39, 391–400.

Hu, L., Lo, I. M. C., Meegoda, J. N., 2006. Numerical analysis and centrifugal modeling of LNAPLs transport in subsurface system. Progress in Natural Science. 16 ,4, 416-424.

Jawitz, J.W., Annable, M.D., Rao, P.S.C., 1998. Miscible fluid displacement stability in unconfined porous media: Two-dimensional flow experiments and simulations. J. Contam. Hydrol. 31, 211–230.

Jellali, S., Benremita, H., Muntzer, P., Razakarisoa, O., Schafer, G., 2003. A large-scale experiment on mass transfer of trichloroethylene from the unsaturated zone of a sandy aquifer to its interfaces. J. Contam. Hydrol. 60(1-2), 31-53.
Jury, W.A., Russo, D., Streile, G., El Abd, H., 1990. Evaluation of volatilization by organic chemicals residing below the soil surface. Water Resour. Res. 26, 13-20.

Kerfoot, H.B., 1994. In situ determination of the rate of unassisted degradation of saturated-zone hydrocarbon contamination. J. Air and Waste Management Association. 44, 7, 877-880.

Khan, F.A., Puls, R.W., 2002. In situ abiotic detoxification and immobilization of hexavalent chromium. Ground Water Monit. Remediat. 23, 77–84.

Klenk, I.D., Grathwohl, P., 2002. Transverse vertical dispersion in groundwater and the capillary fringe. J. Cont. Hydrol. 58 (1-2), 111-128.

Lahvis, M.A., Baehr, A.L., Baker, R.J., 1999. Quantification of aerobic biodegradation and volatilization rates of gasoline hydrocarbons near the water table under natural attenuation conditions. Water Resour. Res. 35,753–765.

Lassin, A., Azaroual, M., Mercury, L., 2005. Geochemistry of unsaturated soil systems: Aqueous speciation and solubility of minerals and gases in capillary solutions. Geochim. Cosmochim. Acta. 69, 22, 5187-5201.

Lehmann, P., Stauffer, F., Hinz, C., Dury, O., Fluehler, H., 1998. Effect of hysteresis on water flow in a sand column with a fluctuating capillary fringe. J. Cont. Hydrol. 33, 81–100.

Lord, D. L., Hayes, K. F., Demond, A. H., Salehzadeh, A., 1997a. Influence of organic acid solution chemistry on subsurface transport properties. 1. Surface and interfacial tension. Environ. Sci. Technol., 31, 2045-2051.

Lord, D. L., Demond, A. H., Salehzadeh, A., Hayes, K. F., 1997b. Influence of organic acid solution chemistry on subsurface transport properties. 2. Capillary pressure- saturation. Environ. Sci. Technol., 31, 2052-2058.

McCarthy, K.A., Johnson, R.L., 1993. Transport of volatile organic compounds across the capillary fringe. Water Resour. Res. 29, 6, 1675-1684.

Neu, T.R., 1996. Significance of bacterial surface-active compounds in interaction of bacteria with interfaces. Microbiol. Rev. 60, 151-166.

Olsson, Å., Grathwohl, P., 2007. Transverse dispersion of non-reactive tracers in homogeneous porous media: a new nonlinear relationship to predict dispersivity. J. Cont. Hydrol. 92, 149-161.

Ostendorf, D.W., DeGroot, D.J., Pollock, S.J., 1995. Aerobic acetate degradation near the capillary-fringe off roadside soil—Field simulations from soil microcosms. J. Environ. Qual. 24,334–342.

Pantazidou, M., Sitar, N., 1993. Emplacement of nonaqueous liquids in the vadose zone. Water Resour. Res. 29, 705 – 722.

Rainwater, k., Mayfield, M.P., Heintz, C., Claborn, B.J., 1993. Enhanced in situ biodegradation of diesel fuel by cyclic vertical water table movement : preliminary studies. Water Environ. Res. 65, 717-725.

Rockhold, M.L., Yardwood, R.R., Selker, J.S., 2004. Coupled microbial and transport processes in soils. Vadose Zone J., 3, 368-383.

Ronen, D., Berkowitz, B., and Magaritz, M., 1989. The development and influence of gas bubbles in phreatic aquifers under natural flow conditions. Transp. Porous Media. 4,295–306.

Ronen, D., Scher, H., Blunt, M., 1997. On the structure and flow processes in the capillary fringe of phreatic aquifers. Transp. Porous Media. 28,159–180.

Ronen, D., Scher, H., Blunt, M., 2000. Field observations of a capillary fringe before and after a rainy season. J. Cont. Hydrol. 44,103–118.

Russo, D., Jury, W.A., Butters, G.L., 1989. Numerical analysis of solute transport during transient irrigation: 1.The effect of hysteresis and profile heterogeneity. Water Resour. Res. 25, 10, 2109-2118.

Schaap, M.G., Leij, F.J., 1998. Database-related accuracy and uncertainty of pedotransfer functions. Soil. Sci. 163, 765-779.

Silliman, S.E., Berkowitz, B., Simunek, J., van Genuchten, M. th., 2002. Fluid flow and chemical migration within the capillary fringe. Ground Water, 40,1, 76-84.

Sinke, A.J.C., Dury, O., Zobrist, J., 1998. Effects of a fluctuating water table: column study on redox dynamics and fate of some organic pollutants. J. Cont. Hydrol. 33, 231-246.

Slavich, P.G., Petterson, G.H., Griffin, D., 2002. Effects of irrigation water salinity and sodicity on infiltration and lucerne growth over a shallow water table. Aust. J. Exp. Agric. 42, 281–290.

Thibodeaux, L.J., 1979. Chemodynamics, Environmental Moverment of Chemicals in Air. Water and Soil. Wiley, New York, NY,501 pp.

Van Genuchten, M.T., 1980. A closed form equation for predicting the hydraulic conductivity of unsaturated soils. Soil Sci. Soc. Am. J. 44, 892-898.

Yarwood, R.R., Rockhold, M.L., Niemet, M.R., Selker, J.S., Bottomley, P.J., 2006. Impact of microbial growth on water flow and solute transport in unsaturated porous media. Water Resour. Res. 42, W10405, doi:10.1029/2005WR004550.

Zaidelman, F.R., Shvarov, A.P., Pavlova, E.B., Golovin, S.N., 1997. Rate of biochemical decomposition of organic matter in drained peaty soils at different sanding modes. Eurasian Soil Sci. 30, 1024–1032.

Zitometer, D.H., Speece, R.E., 1993. Sequential environments for enhanced biotransformation of aqueous contaminants. Environ. Sci. Technol. 27, 226-244.

3. Physical properties of the capillary fringe

3.1 Introduction

Horizontal flow above the water table has been reported in some experiments (e.g., Silliman et al., 2002) and numerical models (Shamsai and Narasimhan, 1991; Wise et al., 1994; Boufadel et al., 1999; Romano et al., 1999; Ronen et al., 1997). Textbooks on groundwater hydrology virtually ignore the role of the CF in flow and transport. Except near regions of discharge to surface water bodies, fluid flow and chemical transport in the subsurface are usually conceptualized as primarily vertical in the unsaturated zone, with transition to fully three-dimensional flow below the water table (Berkowitz, 2004). This chapter focuses on the physical properties of the capillary fringe and gives a theoretical analysis of the horizontal flow above the water table, which is normally less investigated in textbooks, and its potential implication on soil remediation.

The reason why we are interested in the horizontal flow above the water table in general instead of just looking at the flow conditions within the capillary fringe is due to the difficulty in defining the upper limit of the capillary fringe. Although exact terminology varies, most textbooks refer to the CF as the thin zone above the water table with essentially 100% water saturation (as low as 75–85%, depending on the textbook), but with air-entry pressure less than that required to penetrate the water table (e.g., Bear, 1972; de Marsily, 1986; Domenico and Schwartz, 1990; Fetter, 1992). So depending on the processes of interest, some researchers restrict their definition of the capillary fringe only to the part where the water is fully saturated by tension and exclude it wholly from the vadose zone. This is more common among those who are addressing solute transport and water flow (Gillham, 1984; Abdul and Gillham, 1984, 1989). Others define the capillary fringe as both the fully saturated and unsaturated portions above the water table. This is the preferred definition among those who are dealing with the remediation of salt-affected soils as well as those investigating the vapor phase of soil processes and bioremediation. It is not uncommon to see the capillary fringe treated as a boundary condition separating the water table from the unsaturated zone, without defining it as a significant part of either. Although there is not a consistent definition of the upper boundary of the

capillary fringe in reality, we can easily find the water table from gauge pressure =0. In addition, if the capillary fringe is only defined as the tension saturated zone, then the capillary fringe will behave just like the water below the water table. This part should also be considered in a model of saturated groundwater flow (Parlange and Brutsaert, 1987). We can treat it as an upward extension of the water table. As in most cases the compressibility of water is neglected.

Figure 3.1 shows some physical properties of water in soil.

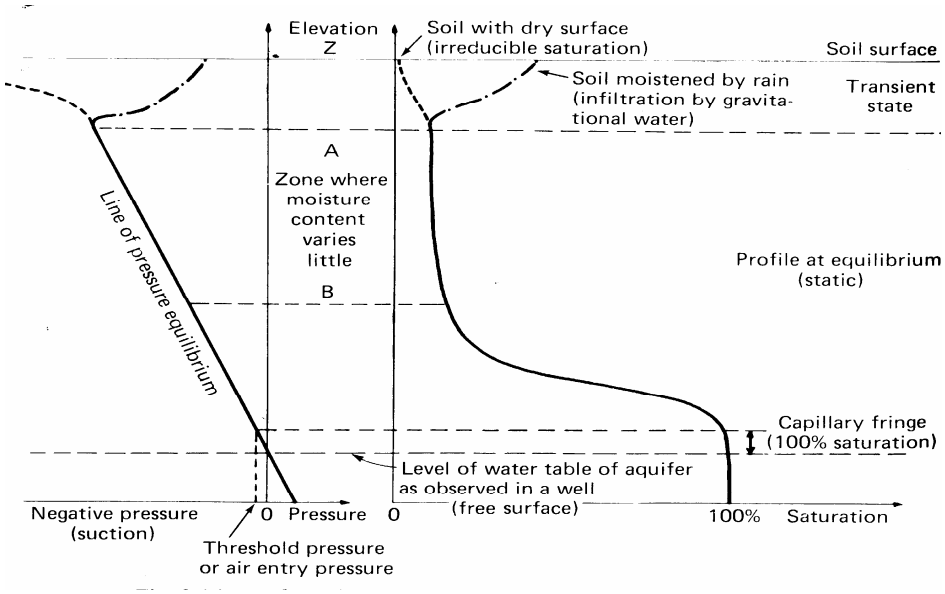

Figure 3.1 Saturation and pressure profiles (from de Marsily, 1986)

As can be seen from Figure 3.1, the capillary fringe is defined here as the tension saturated zone and the water content within the CF is 100%. The water content decreases continuously from the upper boundary of the CF until it reaches residual saturation. There exist some empirical expressions for the pressure and the water content in the unsaturated part, e.g., the van Genuchten (1980), the Brooks & Corey (1964) and modified Mualem-van Genuchten models, in which constant air entry pressure is introduced to account for the near saturated flow within the capillary fringe.

3.2 Hydraulic head above the water table

The hydraulic head at a point *Z* of an incompressible fluid subjected only to gravity is defined by the following relationship:

$$h = \frac{u^2}{2g} + \frac{p}{\rho g} + z \qquad [3.1]$$

u is the real velocity at Z; z is the elevation and p is the pressure.

In porous media, the real velocities are always very slow, and we are justified in omitting the term for dynamic head $\frac{u^2}{2g}$ (de Marsily, 1986), which reduces the hydraulic head to

$$h = \frac{p}{\rho g} + z \qquad [3.2]$$

In Figure 3.1 the line of pressure equilibrium is linearly decreasing from the bottom of the aquifer to the horizontal dashed line A, while the elevation head z increases linearly upward from the bottom of the aquifer if we take the bottom of the aquifer as a reference. Thus the sum of pressure head and elevation head does not change in the vertical direction from the bottom of the aquifer to the dashed line A, i.e., h is not a function of z and the same mean horizontal gradient is applied in both the unsaturated and saturated zone.

3.3 Extended Darcy's law for flow in unsaturated media

Buckingham (1907) extended Darcy's law to describe unsaturated media as

$$q = -K(\theta)\nabla h \qquad [3.3]$$

The hydraulic conductivity, $K(\theta)$, is a function of water content. Figure 3.2 shows how hydraulic conductivity changes with respect to the moisture content, according to an empirical expression (e.g., van Genuchten, 1980; Mualem, 1976; Brooks and Corey, 1964).

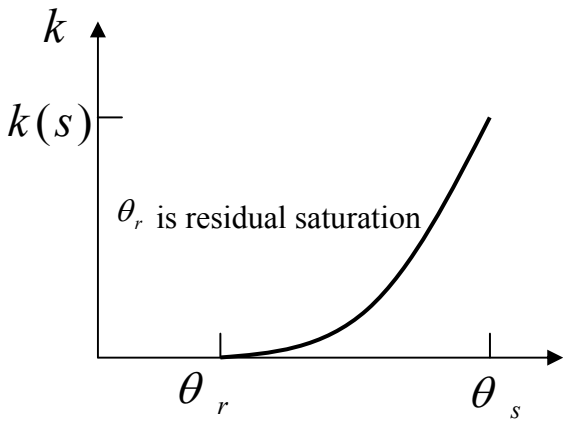

Figure 3.2 Hydraulic conductivity versus moisture content

As this figure shows, as long as the water content is higher than the residual saturation, the hydraulic conductivity is greater than zero.

3.4 Horizontal flow velocity above the water table

Based on the above, the hydraulic head and the extended Darcy's law will result in a horizontal velocity profile in the CF like the one shown in Figure 3.3. We can see in this figure a continuous decrease in horizontal velocity in the unsaturated part. This decrease is very quick due to the rapid decrease of hydraulic conductivity with the water content as shown in Figure 3.2.

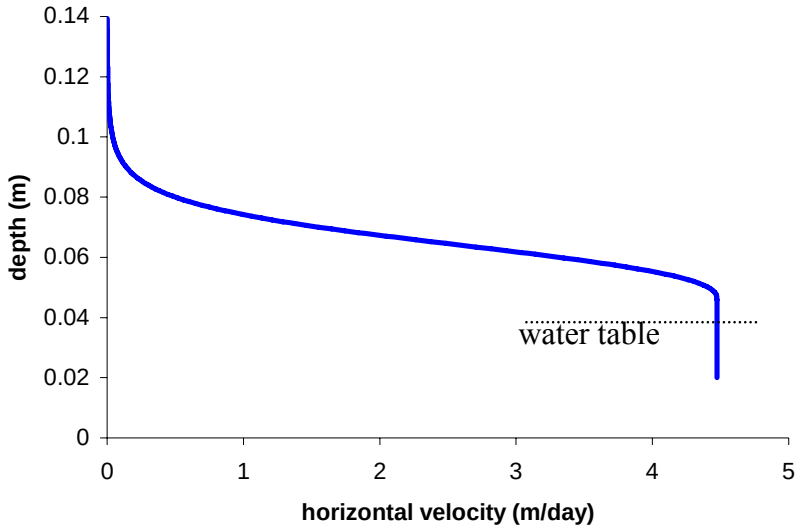

Figure 3.3 Horizontal velocity above the water table (modelling result from Min3p)

3.5 Accumulation of reaction product within the unsaturated capillary fringe

Due to the lower horizontal velocity in the unsaturated part, the contaminants that are transported or produced there can not be transported away as fast as they are in the fully-saturated part. Therefore there is an accumulation of some contaminants within the unsaturated capillary fringe, as can be seen in the reactive transport modelling result of oxygen across the capillary fringe in Figure 3.4. The electron donor used here is sodium dithionite, the electron acceptor is oxygen, and the reaction product is sodium sulfate. After reaching a steady state in the fully saturated part the sodium

sulfate formation rate equals the rate of transport. The concentration profile does not change with time, but as the formation rate is greater than the rate of transport in the unsaturated part, the reaction product accumulates there. From Figure 3.4 we can see that after 5 hours the concentration profiles of electron donor and acceptor do not change; this is also the case for the concentration profile of reaction product in the saturated part where the red and blue lines fall together. But it takes much longer for the concentration of reaction product in the unsaturated part to reach steady state. The reaction product is constantly 'growing' upward into the unsaturated part with time.

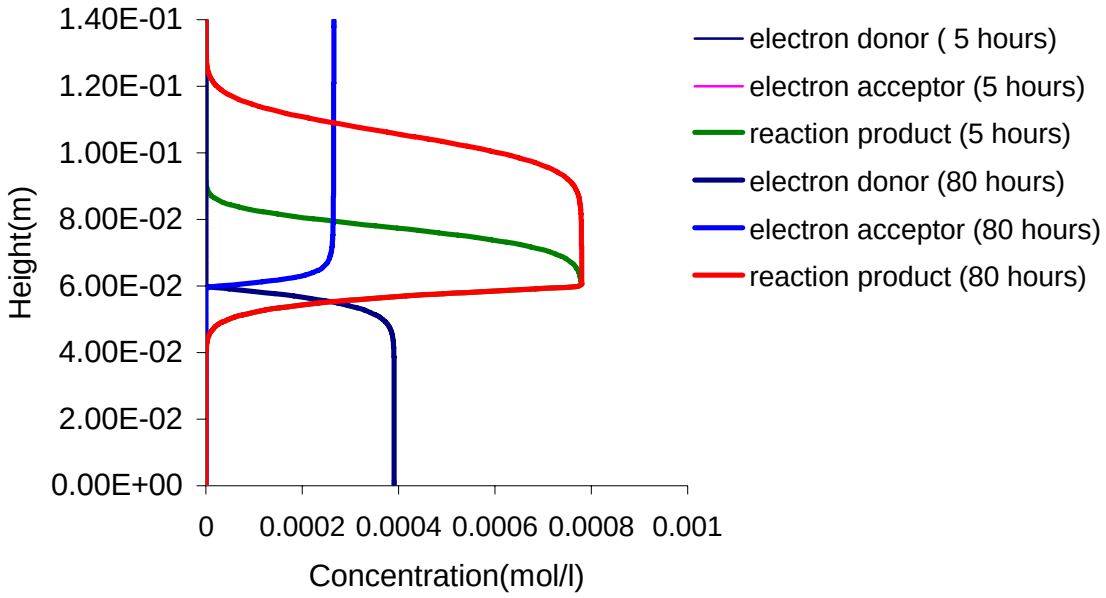

Figure 3.4 Vertical concentration profiles of reactants and product after 5 and 80 hours.

3.6 Independence of the maximum product concentration on the concentration of the electron acceptor

The dependences of the maximum reaction product concentration on the concentration of electron donor and electron acceptor after steady state are shown in Figure 3.5 and Figure 3.6.

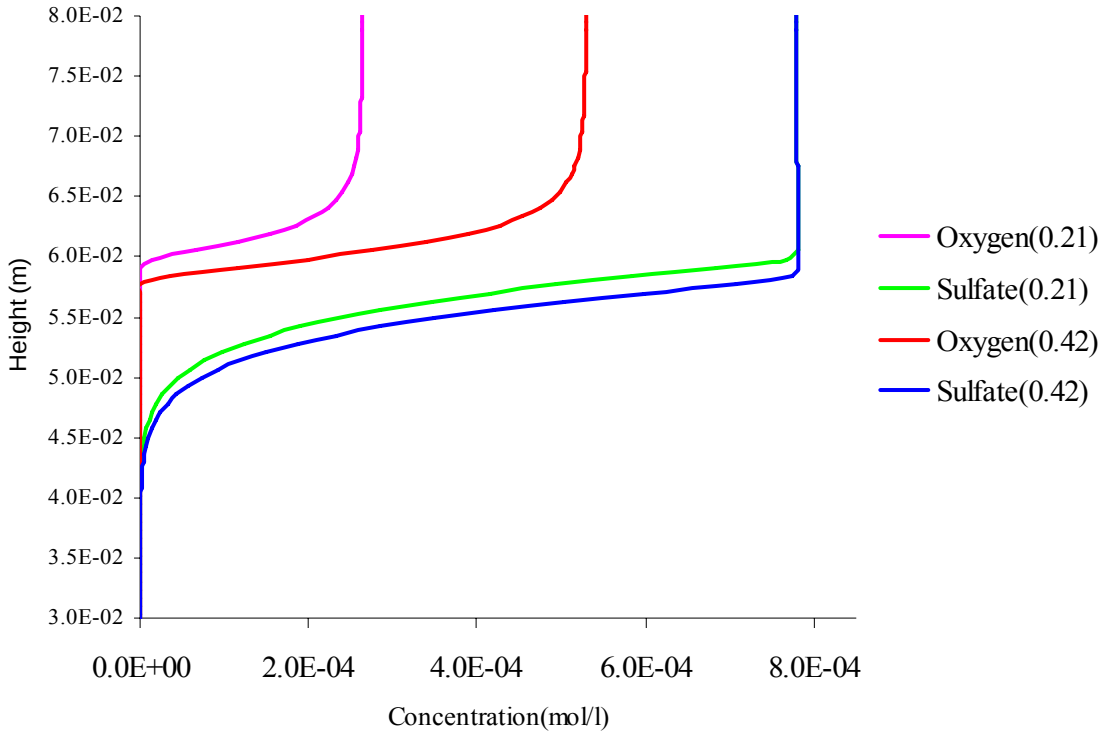

Figure 3.5 sulfate concentration profiles under oxygen partial pressure 0.21 and 0.42

Figure 3.5 shows that doubling the oxygen partial pressure will cause the oxygen front to go deeper, but the maximum sulfate concentration will be still unaffected, which indicates that the maximum sulfate concentration doesn't depend on the oxygen partial pressure.

In contrast to oxygen, if we double the concentration of dithionite, as is shown in Figure 3.6, then the maximum sulfate concentration is also doubled, which indicates the maximum concentration of reaction product is proportional to the concentration of electron donor. These results will be further explained by the analytical solutions in the next chapter.

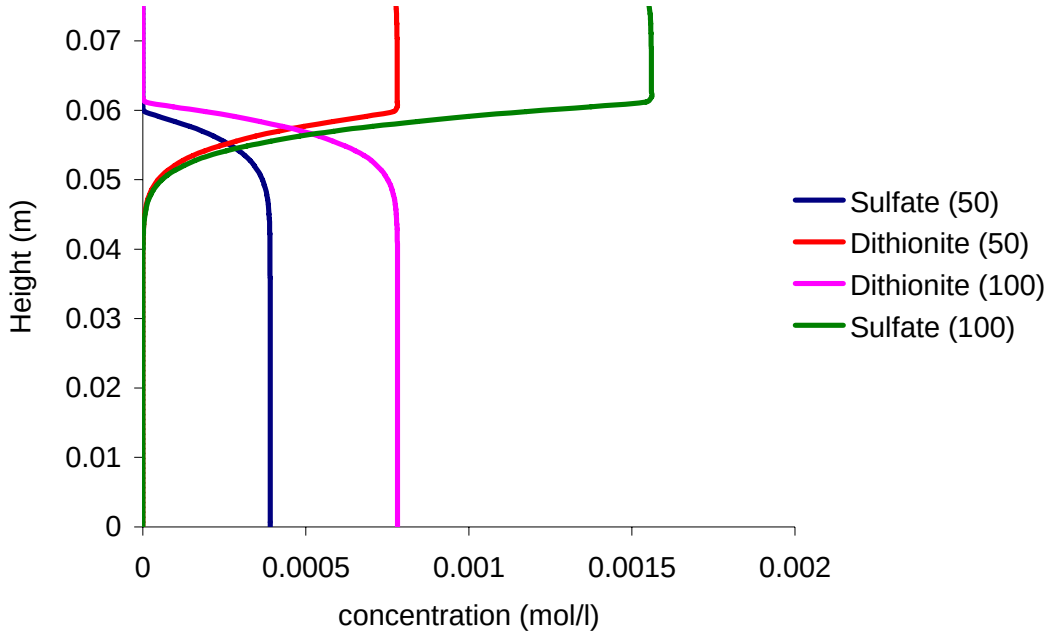

Figure 3.6 Sulfate concentration profiles under dithionite concentration 50 and 100 mg/l

3.7 The transport of oxygen from the air into the water

Gas-phase diffusion in the vadose zone differs from the diffusion through free air. Solid and liquid obstacles reduce the cross sectional area and increase the mean path length for compounds diffusing in soils. The effective diffusion coefficient, D_e, which accounts for the reduction in the diffusion effective cross-sectional area and the increased path length in soils, is used to calculate diffusive gas flux in the vadose zone from concentration gradient according to Fick's first law or to interpret steady-state vapour concentration profile (Werner et al., 2004; Wang et al., 2003).

The effective diffusion coefficient in the gaseous phase is usually calculated by an empirical correlation given by Millington (1959)

$$D_e = D_{air} \frac{(n-\theta)^{10/3}}{n^2} \qquad [3.4]$$

where n is the overall porosity of the medium, θ the volume water content of the medium and D_{air} the diffusion coefficient in free air.

For the calculation of the effective diffusion coefficient a number of other studies have also been conducted (e.g., Marshall, 1959; Currie, 1960; Millington, 1959; Millington and Quirk, 1961; Moldrup et al., 1997, 2000). For volatile organic compounds, volatilization from multicomponent organic liquids, and diffusion in unsaturated porous media Wang et al. (2003) found that the Moldrup et al. (2000) model more accurately predicted the effective diffusion coefficient D_e for a wide range of soil water contents.

With the increase of water saturation from the soil surface to groundwater, the effective oxygen gaseous diffusion coefficient decreases. At the same time the horizontal velocity increases and the transverse vertical mechanical dispersion becomes important in mass transfer of oxygen. As the green line in Figure 3.7 shows, the minimal mass transfer coefficient lies several centimetres above the water table. Depending on the diffusion coefficient and the horizontal flow velocity, this location can shift.

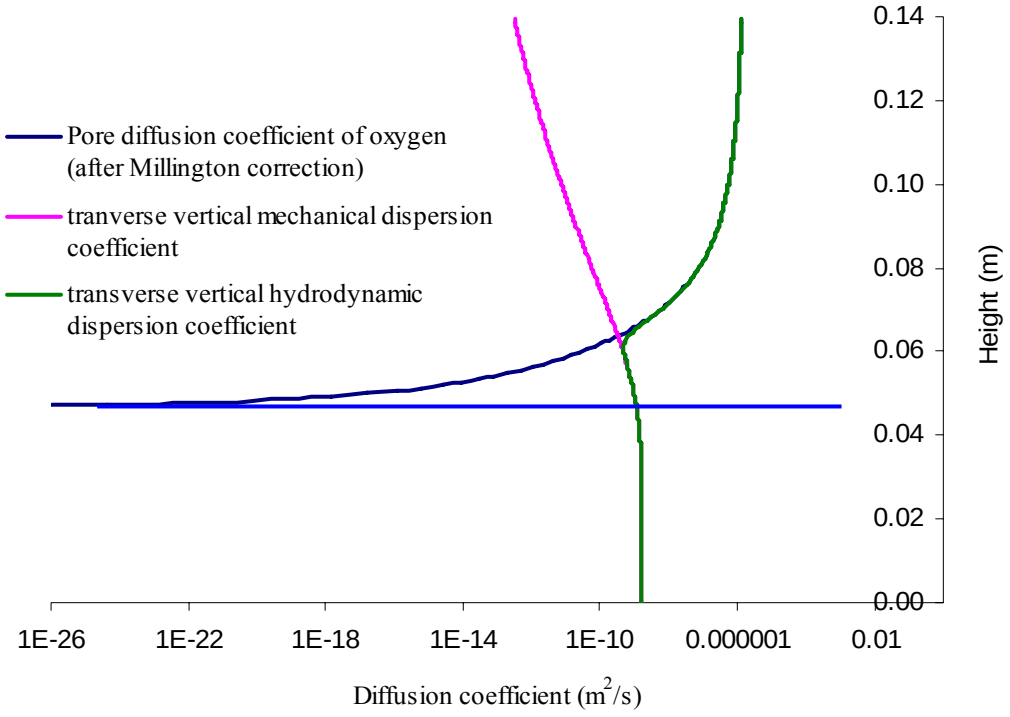

Figure 3.7 Diffusion and dispersion coefficients distribution for a soil vertical profile

Figure 3.8 and 3.9 are modelling results based on the Millington-Quirk correction. As can be seen in Figure 3.8 and 3.9, for the oxygen transport (both reactive and non-

reactive) from the air into the groundwater the oxygen concentration has almost no gradient above the 85% water saturation line, which means the gaseous phase oxygen is continuous above this line and the less saturated part does not limit the downward diffusion of oxygen. As soon as the oxygen reaches the 85% saturation line the effective oxygen diffusion coefficient is not large enough for the gaseous oxygen to diffuse freely and the concentration gradient starts to develop rapidly there. This will be further verified by the experimental result in chapter 5.

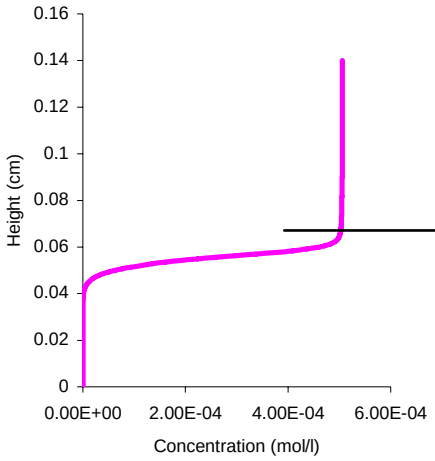

Figure 3.8 Oxygen profile after reaching steady state

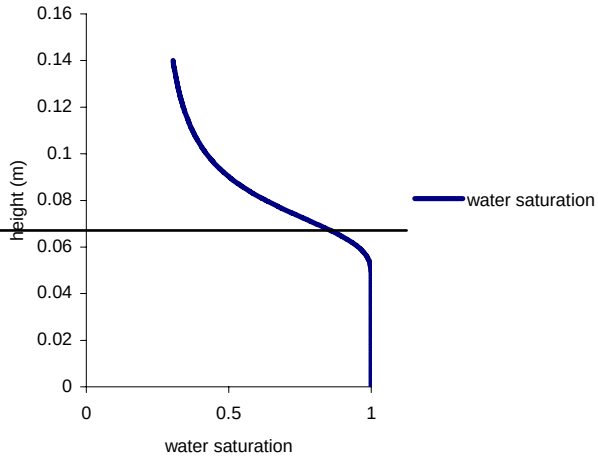

Figure 3.9 Water saturation profile

3.8 Definition of the capillary fringe

Now, to come back to the definition of the capillary fringe, if we are just interested in the oxygen transport from the air to the groundwater, then the important part is from the water table to the 85% saturation line, i.e. where the gradient develops rapidly: we will therefore define this part as the capillary fringe. The part above the 85% saturation line (it may deviate a little bit from 85% depending on which model is used for the tortuosity correction) offers almost no resistance to this transfer process. In the case of soil remediation, however, the accumulation or entrapment of some pollutants in the less saturated part (due to the lower horizontal velocity and capillary entrapment) will force us to extend the capillary fringe from the 85% saturation line to the location where the horizontal velocity equals 0, i.e., the water content reaches residual saturation.

References

Abdul, A.S., Gillham, R.W., 1984. Laboratory studies of the effect of the capillary fringe on stream-flow generation. Water Resour. Res. 20, no.6:691-698

Abdul, A.S., Gillham, R.W., 1989. Field studies of the effect of the capillary fringe on streamflow generation. Journal of hydrology. 112 (1989) 1-18.

Bear, J. 1972. Dynamics of fluids in porous media. Elsevier, New York.

Berkovitz, B., Silliman, S.E., Dunn, A.M., 2004. Impact of the Capillary Fringe on Local Flow, Chemical Migration, and Microbiology. Vadose Zone Journal 3:534-548.

Boufadel, M.C., Suidan, M.T., Venosa, A.D., Bowers, M.T., 1999. Steady seepage in trenches and dams: effect of capillary flow. J. Hydraulic Eng.-ASCE 125, no. 3:286-294.

Brooks, R.H., Coery, A.T., 1964. Hydraulic properties of porous media. Hydrology paper, Colorado State University, Ft. Collins.

Buckingham, E., 1907. Studies in the movement of soil moisture. Bull. 38, USDA Bureau of Soils, Washington, DC, 29-61.

Currie, J.A., 1960. Gaseous diffusion in porous media. II. Dry granular materials. Br. J. Appl. Phys. 11:318-324.

de Marsily, G., 1986. Quantitative hydrogeology—Groundwater hydrology for engineers. Academic Press, San Diego, CA.

Domenico, P.A., and Schwartz, F.W., 1990. Physical and chemical hydrogeology. John Wiley and Sons, New York.

Fetter, C.W., 1992. Applied hydrogeology. Prentice Hall, Englewood Cliffs, NJ.

Gillham, R.W., 1984. The capillary fringe and its effect on water-table response. Journal of Hydrology, 67:307-324.

Jury, A., Gardner, W. R., Gardner, W.H., 1991. Soil Physics, John Wiley and Sons.

Marshall, T. J., 1959. The diffusion of gas through porous media. J. Soil Sci. 10:79-82.

Mayer, K.U., 1999. A numerical model for multicomponent reactive transport in variably saturated porous media. Ph.D. thesis, Department of Earth Sciences, University of Waterloo.

Millington, R.J., 1959. Gas diffusion in porous media. Science 130:100-102.

Millington, R. J., Quirk, J.P., 1961. Permeability of porous solids. Trans. Faraday Soc. 57: 1200-1207.

Moldrup, P., Olesen, T., Gamst, J., Schjønning, P., Yamaguchi, T., Rolston, D.E., 2000. Predicting the gas diffusion coefficient in repacked soil: Water-induced linear reduction model. Soil Sci. Soc. Am. J. 64:1588–1594.

Moldrup, P., Olesen, T., Rolston, D.E.,Yamaguchi, T., 1997. Modeling diffusion and reaction in soil: VII. Predicting gas and ion diffusivity in undisturbed and sieved soil. Soil Sci. 162:632–640.

Mualem, Y., 1976. A new model for predicting the hydraulic conductivity of unsaturated porous media. Water Resour. Res. 12:513-522.

Parlange, J.-Y., Brutsaert, W., 1987. A capillary correction for free surface flow of groundwater. Water Resour. Res. 23, no. 5:805-808.

Romano, C.G., Frind, E.O., Rudolph, D.L., 1999. Significance of unsaturated flow and seepage faces in the simulation of steady-state subsurface flow. Ground water. 37, no. 4: 625-632.

Ronen,D., Scher,H., Blunt,M.J., 1997. On the Structure and Transport Properties in the Capillary Fringe of Phreatic Aquifers, Transport in Porous Media. Vol: 28, Pages: 159 – 180.

Schaap, M.G., van Genuchten, M. Th., 2006. A Modified Mualem-van Genuchten formulation for improved description of the hydraulic conductivity near saturation, Vadose Zone Journal 5: 27-34.

Shamsai, A., Narasimhan, T.N., 1991. A numerical investigation of free surface-seepage face relationship under steady state flow conditions. Water Resour. Res. 27, no.3:409-421.

Silliman, S.E., Berkowitz, B., Simunek, J., van Genuchten, M.Th., 2002. Fluid flow and chemical migration within the capillary fringe. Ground Water 40:76–84.

van Genuchten, M.Th. 1980. A closed-form equation for predicting the hydraulic conductivity of unsaturated soils. Soil Sci. Soc. Am. J. 44:892–898.

Wang, G., Reckhorn, S.B.F., Grathwohl, P., 2003. Volatilization of VOC from multicomponent mixtures in unsaturated porous media. Vadose Zone Journal, 692 – 701.

Werner, D., Grathwohl, P., Höhener, P., 2004**.** Review of field methods for the determination of the tortuosity and effective gas-phase diffusivity in the vadose zone. 3:1240-1248.

Wise, W.R., Clement, T.P., Molz, F.J., 1994. Variably saturated modeling of transient drainage-Sensitivity to soil properties. J. Hydrol. 161, nos. 1-4: 91-108.

4. Analytical solutions of oxygen spatial distribution and the length of the electron donor plume

4.1 Introduction

Locally at the air-water interface, equilibrium is reached between the oxygen in the air and in the water according to Henry's law, and since gas phase transport of oxygen is fast, the aqueous oxygen concentration at the top of the capillary fringe can be assumed to be constant. Therefore, the transport of oxygen across the capillary fringe can be treated as diffusion into a semi-infinite medium analogous to the dissolution of NAPL pools (Johnson and Pankow, 1992; Eberhardt and Grathwohl, 2002) as shown for the non-reactive case by Klenk and Grathwohl (1999). For the dissolution of NAPL pools with a first order reaction, Chrysikopoulos et al. (2003) gave an analytical solution by solving the governing partial differential equation by Laplace transformation. Due to the same governing equations and boundary conditions this analytical solution may also be used to describe the oxygen transfer across the capillary fringe, assuming first order reactions of a compound. However, this does not describe reactive transport with fast reactions ("quasi instantaneous") where the overall reaction rate depends on the mixing rate of the reaction partners as shown in many studies on natural attenuation of organic compounds in groundwater (Cirpka et al., 2006; Liedl et al, 2005). So far no analytical solution exists to describe the NAPL pools dissolution nor the transfer of oxygen across the capillary fringe with an instantaneous reaction, i.e. the reaction rate constant λ does not limit the overall reaction rate, which in turn depends on mass transfer rates of reaction partners. In our study, an analytical solution that assumes a fully saturated capillary fringe is derived to model the reactive transfer of oxygen across the capillary fringe with an instantaneous reaction. The analytical solution was compared to numerical simulations with MIN3P (Mayer, 1999; Mayer et al., 2002) to identify the influence of the variable water content in the capillary fringe on the oxygen transfer.

4.2 Conceptual model

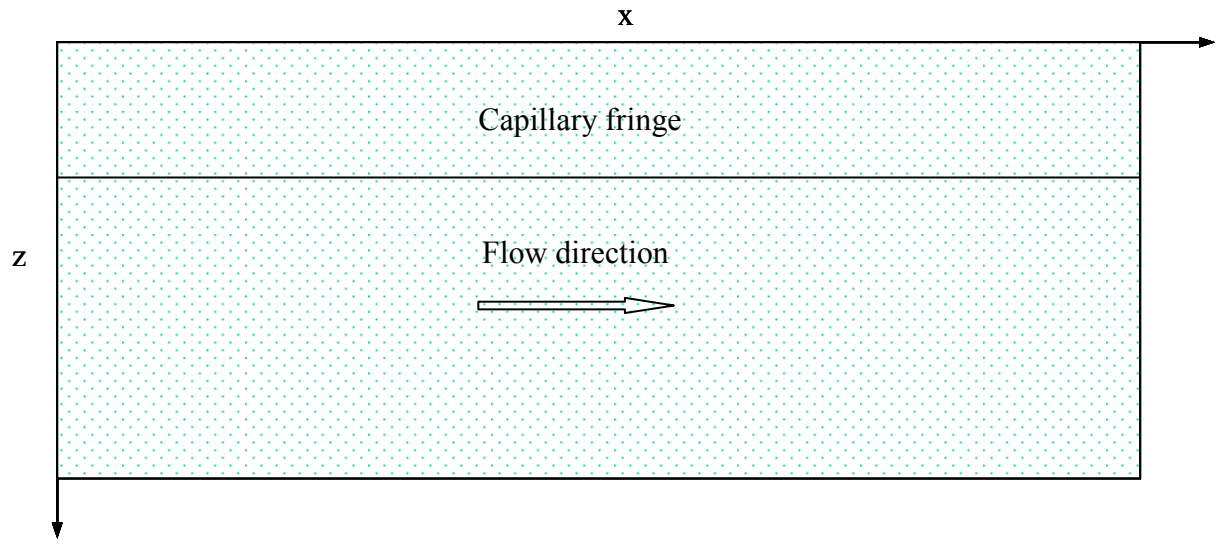

Figure 4.1 Illustration of the capillary fringe and saturated zone in the conceptual model

Figure 1 shows the scenario used in the model system. It is a two dimensional tank. We assume that the gas phase in the unsaturated zone is continuous, and at the upper limit of the capillary fringe the concentration of oxygen is kept constant. The oxygen concentration (electron acceptor) in water is given by

$$C_{A0} = \frac{P_{O2}}{H} \qquad [4.1]$$

where P_{o2} is the partial pressure of oxygen in the air and H is Henry's law constant (769.23 l.atm/mol at 298K and 594.7 l.atm/mol at 283K). At x=0 the oxygen concentration is zero.

The electron donor B (non volatile) with concentration C_{B0} is continuously injected into the system from the inlet part (left) at a constant rate. Due to the oxygen far away from the bottom of the tank we assume a remote boundary condition for A and B, i.e. when z goes to infinity the concentration of B is C_{B0} and the concentration of A is zero.

Furthermore, we assume an instantaneous reaction between oxygen A and the electron donor B which results in a reaction product C (non volatile). The reaction equation and rate expressions are as follows:

$$\begin{array}{l} Y_1 A + Y_2 B \rightarrow C \\ -Y_1\gamma \; -Y_2\gamma \quad \gamma \end{array}$$

Where γ is the rate of the production of C. Y_1 and Y_2 are stoichiometric coefficients for oxygen and electron donor *B* respectively. They can be any positive number, so that this reaction may be applied to reaction with arbitrary stoichiometries.

4.3 Governing transport equations and analytical solutions

After steady state the transport equations of all these three species with concentration C_i are:

$$\frac{\partial C_i}{\partial t} + v\frac{\partial C_i}{\partial x} + w\frac{\partial C_i}{\partial z} = D_x \frac{\partial^2 C_i}{\partial x^2} + D_z \frac{\partial^2 C_i}{\partial z^2} \pm \gamma \qquad [4.2]$$

Where *i* can be A, B and C. *v* and *w* are flow velocities in x and z directions. D_x and D_z are hydrodynamic dispersion coefficients in x and z directions.

We assume parallel flow in the tank. Vertical velocities (groundwater recharge is not taken into account) and longitudinal dispersion ($Pe = \frac{vL}{D_x} >> 1$) are therefore neglected in eq [4.2]. Transport of all species (A, B, C) is by transverse hydrodynamic dispersion and horizontal advection. With the equation [4.2] for A, B and C reduced to:

$$v\frac{\partial C_A}{\partial x} = D_z \frac{\partial^2 C_A}{\partial z^2} - Y_1\gamma \qquad [4.3]$$

$$v\frac{\partial C_B}{\partial x} = D_z \frac{\partial^2 C_B}{\partial z^2} - Y_2\gamma \qquad [4.4]$$

$$v\frac{\partial C_C}{\partial x} = D_z \frac{\partial^2 C_C}{\partial z^2} + \gamma \qquad [4.5]$$

Coupling [4.3] and [4.5], [4.4] and [4.5] results in

$$v\frac{\partial(C_A + Y_1 C_C)}{\partial x} = D_z \frac{\partial^2 (C_A + Y_1 C_C)}{\partial z^2} \quad [4.6]$$

$$v\frac{\partial(C_B + Y_2 C_C)}{\partial x} = D_z \frac{\partial^2 (C_B + Y_2 C_C)}{\partial z^2} \quad [4.7]$$

D_z is commonly defined as:

$$D_z = D_{pore} + \alpha_t v \quad [4.8]$$

D_{pore} denotes the pore diffusion coefficient which according to Boving and Grathwohl (2001) is approximately:

$$D_{pore} \cong nD_{aq} \quad [4.9]$$

Due to the low pore diffusion coefficients, we assume mechanical dispersion dominates over diffusion and D_z is therefore not compound specific.

Boundary conditions for eq [4.7] are:

$$C_B + Y_2 C_C(x = 0, z) = C_{B0} \quad [4.10]$$

$$\frac{\partial(C_B + Y_2 C_C)}{\partial z}|_{z=0} = 0 \quad [4.11]$$

$$C_B + Y_2 C_C(x, z = \infty) = C_{B0} \quad [4.12]$$

With these boundary conditions the analytical solution of eq [4.7] can be easily obtained as follows:

$$C_B + Y_2 C_C = C_{B0} \quad [4.13]$$

Boundary conditions for eq [4.6] are:

$$C_A + Y_1 C_C(x = 0, z) = 0 \quad [4.14]$$

Because *A* and *B* can't coexist, at $z = 0$ where C_A equals C_{A0} the concentration of *B* must be zero. From eq [4.13] we know that the concentration of C_c equals $\frac{C_{B0}}{Y_2}$, so at *z*=0 we have

$$C_A + Y_1 C_C(x, z = 0) = C_{A0} + C_{B0}\frac{Y_1}{Y_2} \qquad [4.15]$$

At the bottom of the modelling domain a remote boundary condition is assumed where

$$C_A + Y_1 C_C(x, z = \infty) = 0 \qquad [4.16]$$

The method of 'combination of variables' (Boltzmann, 1894) yields the solution to eq [4.6]:

$$C_A + Y_1 C_C = (C_{A0} + C_{B0}\frac{Y_1}{Y_2})erfc(\frac{z}{2\sqrt{D_z \frac{x}{v}}}) \qquad [4.17]$$

The location z^* where both the concentrations of *A* and *B* go to zero (the penetration depth of the reaction front) can be obtained as follows:

From eq [4.17] we have

$$C_C = (\frac{C_{A0}}{Y_1} + \frac{C_{B0}}{Y_2})erfc(\frac{z^*}{2\sqrt{D_z \frac{x}{v}}}) \qquad [4.18]$$

and from eq [4.13] we have

$$C_C = \frac{C_{B0}}{Y_2} \qquad [4.19]$$

Comparing eq [4.18] and eq [4.19] we can get

$$z^* = erfc^{-1}(\frac{Y_1 C_{B0}}{Y_1 C_{B0} + Y_2 C_{A0}})2\sqrt{D_z \frac{x}{v}} \qquad [4.20]$$

Where $erfc^{-1}$ is the inverse function of the complimentary error function.

For example, if C_{A0} equals C_{B0}, Y_1 equals Y_2, then $erfc^{-1}(0.5)$ equals 0.477 and the penetration depth is

$$z^* = 0.477 * 2\sqrt{D_z \frac{x}{v}} \approx \sqrt{D_z \frac{x}{v}} \qquad [4.21]$$

Eq [4.13] also suggests that concentration of the reaction product above z* is constant and equals

$$C_C(z \le z^*) = \frac{C_{B0}}{Y_2} = C_{\max} \qquad [4.22]$$

This means that the maximum reaction product concentration just depends on the concentration of the compound in the water *B* (electron donor) and not on the compound in the unsaturated zone *A* (electron acceptor). This verifies the numerical modelling result from Chapter 3.

The concentrations of all these 3 compounds at different depths are shown as follows:

For $z < z^*$ (i.e. location above z^*) $C_B = 0$ and based on eq [4.13] and eq [4.17] we have

$$C_C = \frac{C_{B0}}{Y_2} \qquad [4.23]$$

$$C_A = (C_{A0} + C_{B0}\frac{Y_1}{Y_2})erfc(\frac{z}{2\sqrt{D_z \frac{x}{v}}}) - \frac{Y_1}{Y_2}C_{B0} \qquad [4.24]$$

For $z > z^*$ (i.e. locations below z^*), $C_A = 0$ and based on eq [4.13] and eq [4.17] we have

$$C_C = (\frac{C_{A0}}{Y_1} + \frac{C_{B0}}{Y_2})erfc(\frac{z}{2\sqrt{D_z \frac{x}{v}}}) \qquad [4.25]$$

$$C_A = C_{B0} - (\frac{Y_2}{Y_1}C_{A0} + C_{B0})erfc(\frac{z}{2\sqrt{D_z \frac{x}{v}}}) \qquad [4.26]$$

The vertical dispersive flux at any location x is

$$F(x) = -D_z n \frac{\partial C_A}{\partial z}\bigg|_{z=0} = (C_{A0} + \frac{Y_1}{Y_2}C_{B0})n\sqrt{\frac{D_z v}{\pi x}} \qquad [4.27]$$

By integrating $F(x)$ over the total domain length L, the total flux of component A into the two dimensional system is

$$F_{total} = \int_0^L F(x)dx = (C_{A0} + \frac{Y_1}{Y_2} C_{B0}) n \sqrt{\frac{4D_z vL}{\pi}} \qquad [4.28]$$

For the non-reactive case where $C_{B0} = 0$ and replace v with L/t eq [4.28] reduces to

$$F_{total} = C_{A0} n \sqrt{\frac{4D_z}{\pi t}} L \qquad [4.29]$$

Eq [4.29] agrees with the analytical solution from Klenk and Grathwohl (1999).

4.4 Comparison of the analytical solution with numerical modeling

In order to check the applicability of the analytical solutions described above to a more realistic case of reactive oxygen transport across the capillary fringe a numerical model was set up. The numerical model MIN3P (Mayer, 1999) solves the advection and dispersion equations in the water and accounts for diffusion in the gas phase. This model allows an accurate description of water contents and hydraulic properties in the capillary fringe, i.e. the soil water retention curve $\theta(h)$ and the hydraulic conductivity function $k(\theta)$ (θ is the volumetric water content, h is the pressure head and k is the hydraulic conductivity).

As example reaction we used is the following:

$$0.5\ S_2O_4^{2-} + 0.75\ O_2 + 0.5\ H_2O \rightarrow SO_4^{2-} + H^+$$

$S_2O_4^{2-}$ is the electron donor (B) and O_2 is the electron acceptor (A). The reaction product (C) is SO_4^{2-}. The stoichometric factors Y_1 and Y_2 are 0.75 and 0.5, respectively.

Figure 4.3 shows the vertical concentration profiles (x = 0.6m) obtained from numerical modelling and analytical solution. As can be seen from this figure below z^* the analytical solutions fit the modelling results very well. Sulfate and dithionite concentration profiles obtained from both methods are almost identical. The analytical solutions deviate from the modelling results as the water becomes partially saturated.

This is because the analytical model assumes a fully saturated capillary fringe, whereas the numerical model (Min3p) employs Van Genuchten parameters (van Genuchten, 1980) which assume a gradual decrease of water saturation away from the water table, as is shown in Figure 4.2. All mass transfer parameters used in the numerical simulation are summarized in Table 1.

Table 4.1 Parameters used in the modelling

D_{air} [$m^2 s^{-1}$]	D_{aq} [$m^2 s^{-1}$]	α_l [m]	α_t [m]	v [m/day]	α [m^{-1}]	l	m
2.0E-5	2.0E-9	0.002	0.0003	4.6	30	0.5	3.2

(α, l and m are Van Genuchten parameters)

Horizontal velocity, dispersion, and the diffusion coefficients change with the water saturation and these cause some deviation of the numerical model from the analytical solution which relies on constant transport parameters over the whole depth. The higher the water content the better the analytical solution fits the numerical results. Therefore, for fully water saturated conditions or high water content, for example in the case of coarse grained materials where the capillary fringe is very shallow, the analytical solutions can be applied.

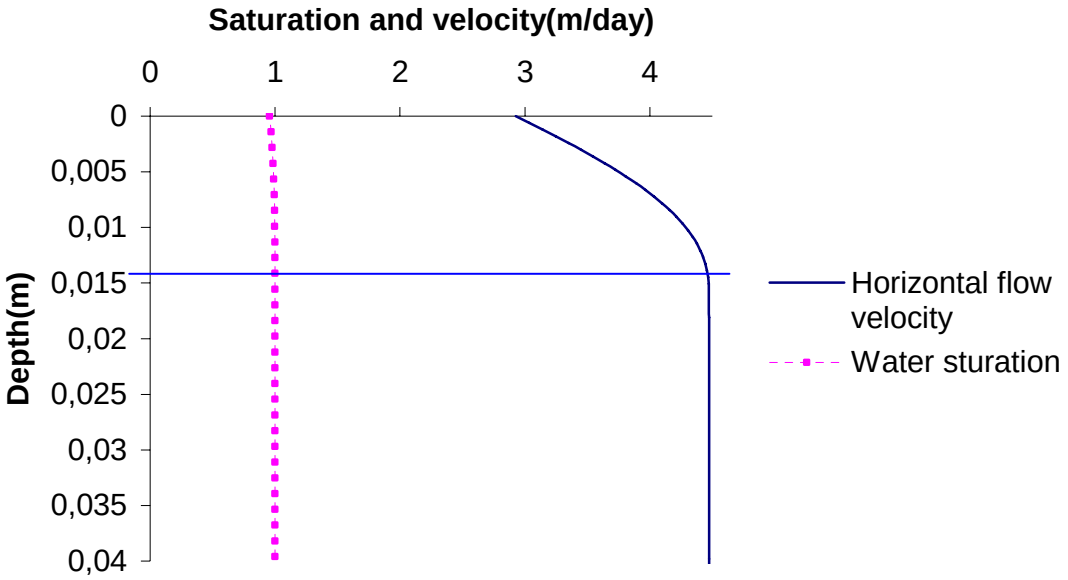

Figure 4.2 Horizontal velocity and water saturation curve at x=0.6m from Van Genuchten model (Horizontal line marks the water table)

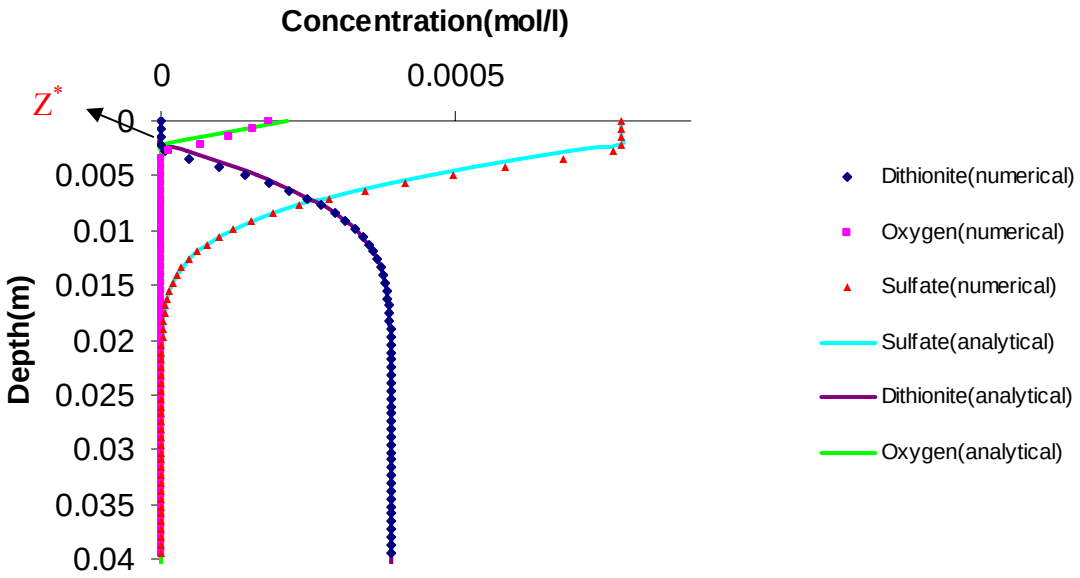

Figure 4.3 Vertical concentration profiles of reactants and product (steady state). The arrow highlights the location where both electron donor and electron acceptor goes to zero.

4.5 Summary

In this study the closed-form analytical solutions describing the reactants and product concentration profiles and also the total oxygen flux into the system after reaching steady state are presented. The analytical solutions verify the modelling results from chapter 3 which show that, above the location where both electron donor and electron acceptor go to zero, the concentration of product is constant and doesn't depend on the concentration of electron acceptor. It only depends on the initial concentration of electron donor and the stoichiometric ratio of electron donor and product. Compared to the non reactive case, the penetration depth of oxygen is decreased and all the reaction terms go to the argument of the inverse function of a complementary error function. These analytical solutions can also be applied to the non-reactive case by simply assigning $C_{B0} = 0$. This simple model can be used in the prediction of reactive oxygen transfer for soil with high water saturation in the capillary fringe or very coarse materials for which the capillary fringe is very thin.

References

Boltzmann, L., 1894. Annalen der Physik und Chemie, 53, 959.

Boving, T, Grathwohl, P. (2001): Matrix diffusion coefficients in sandstones and limestones: Relationship to permeability and porosity.- J. Cont. Hydrol., 53 (1-2), 85-100 .

Chrysikopoulos, C.V., P. Hsuan, M.M. Fyrillas, and K.Y. Lee., 2003. Mass transfer coefficient and concentration boundary layer thickness for a dissolving NAPL pool in porous media. Journal of Hazardous Materials B97, 245–255.

Cirpka, O. A., Olsson, A., Ju, Q. S., Rahman, M. A., Grathwohl, P., 2006. Determination of transverse dispersion coefficients from reactive plume lengths. Ground Water, 44, 212-221.

Eberhardt, C., Grathwohl, P. (2002). Time scales of pollutants dissolution from complex organic mixtures: blobs and pools.- J. Cont. Hydrol., 59, 1-2, 45-66 (Invited paper for Special Issue of J. Cont. Hydrol. on Site Remediation).

Grathwohl, P., 1997. Gefährdung des Grundwassers durch Freisetzung organischer Schadstoffe: Methoden zur Berechnung der in-situ-Schadstoffkonzentration, Grundwasser Zeitschrift der Fachsektion Hydrogeologie, 4/97, 157-166.

Johnson, R.L. and Pankow, J.F., 1992. Dissolution of dense chlorinated solvents into groundwater. 2. Source functions for pools of solvent, Environmental Science & Technology, 26, 5, 896-901.

Klenk, I. and Grathwohl, P., 1999. Sickerwasserprognose bei biologisch abbaubaren Mineralölkohlenwasserstoffen (MKW) in der wasserungesättigten Bodenzone, Forschungsbericht im Auftrag des Umweltbundesamtes (UBA) und des Deutschen Institutes für Normung (DIN), pp. 221.

Klenk, I.D., Grathwohl, P., 2002. Transverse vertical dispersion in groundwater and the capillary fringe Journal of Contaminant Hydrology 58 (1-2), pp. 111-128.

Liedl, R., A. J. Valocchi, P. Dietrich, and P. Grathwohl (2005), Finiteness of steady state plumes, Water Resour. Res., 41, W12501, doi:10.1029/2005WR004000.

Mayer, K.U., 1999. A numerical model for multicomponent reactive transport in variably saturated porous media. Ph.D. thesis, Department of Earth Sciences, University of Waterloo.

Mayer, K. U., E. O. Frind, and D. W. Blowes (2002), Multicomponent reactive transport modeling in variably saturated porous media using a generalized formulation for kinetically controlled reactions, Water Resour. Res., 38(9), 1174, doi:10.1029/2001WR000862.

van Genuchten, M.Th. 1980. A closed-form equation for predicting the hydraulic conductivity of unsaturated soils. Soil Sci. Soc. Am. J. 44:892–898.

Appendix: Finite boundary conditions - the length of the steady state plume

The boundary condition eq [4.16] is a remote boundary condition that holds true as long as the reaction front is far away from the bottom of the aquifer as is the case in the tank experiment in the next chapter. However, since this assumes that the reaction front can't reach the bottom of the aquifer, we can't determine the length of the electron donor plume from these solutions. As the distance in the flow direction increases, the influence of the bottom impervious layer can't be neglected any longer.

By changing the boundary condition in eq [4.16] to a no flux boundary at the bottom of the aquifer we can solve this problem in an alternative to Liedl et al. (2005).

The procedure is as follows.
Assuming a no flux boundary at the bottom of the aquifer the boundary condition [4.16] changes to:

$$\frac{\partial(C_A + Y_1 C_C)}{\partial z}\Big|_{z=M} = 0 \qquad [4.16^*]$$

where M is the thickness of the aquifer. All the other boundary conditions stay the same.

The solution to eq [4.6] under such boundary conditions can be solved by adding an identical image source at the location where $z = 2M$ as is shown in Figure 4.a. The additional source (dashed arrow) is located at the mirror image to the original source with the mirror located at the no flux boundary $z=M$. The shape of the reaction front for the image source is shown as a dashed line. Its shape is identical to the original source, but its peak is shifted from $z=0$ to $z=2M$. The shift can be accomplished by forcing the complimentary error function in eq [4.17] to be one at $z=2M$, *i.e.* making the argument zero at $z=2M$.

$$(C_A + Y_1 C_C)\Big|_{image} = (C_{A0} + C_{B0}\frac{Y_1}{Y_2})erfc(\frac{2M - z}{2\sqrt{D_z \frac{x}{v}}}) \qquad [a]$$

So the solution is the sum of the real source and image source, which is:

$$C_A + Y_1 C_C = (C_{A0} + C_{B0}\frac{Y_1}{Y_2})erfc(\frac{z}{2\sqrt{D_z \frac{x}{v}}}) + (C_{A0} + C_{B0}\frac{Y_1}{Y_2})erfc(\frac{2M - z}{2\sqrt{D_z \frac{x}{v}}}) \qquad [b]$$

As can be seen from eq (b), if z is very small in comparison to M, the argument of the complimentary error function in the second term is much greater than in the first term; therefore the influence of the image source can be neglected

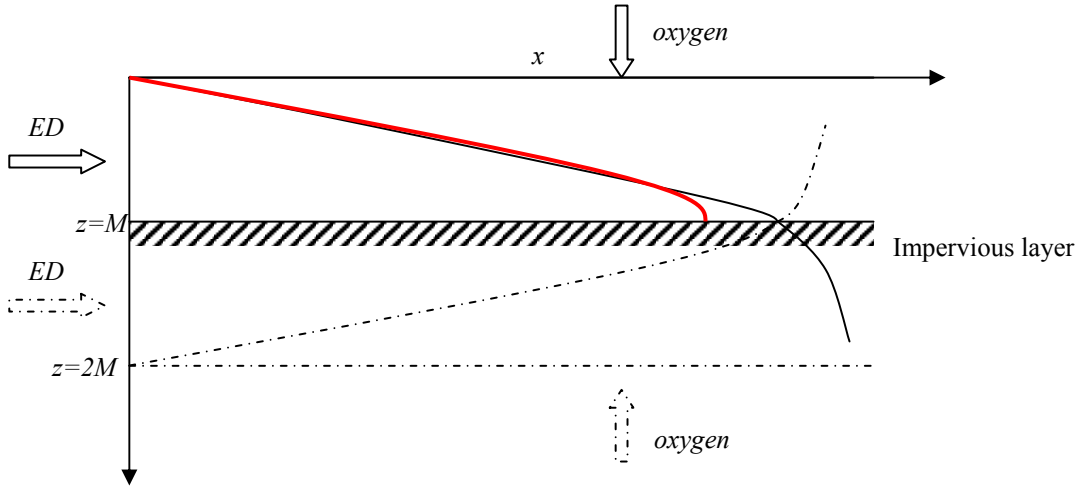

Figure 4.a. Adding an image source (dashed lines) to the real source to create a solution (red) in the real domain ($0<z<M$) to satisfy the boundary condition [16*].

correspondingly eq [4.18] changes to

$$C_C = (\frac{C_{A0}}{Y_1} + \frac{C_{B0}}{Y_2})(erfc(\frac{z^*}{2\sqrt{D_z \frac{x}{v}}}) + erfc(\frac{2M - z^*}{2\sqrt{D_z \frac{x}{v}}})) \qquad [c]$$

Combining eq [c] and eq [4.19] we have

$$\frac{C_{B0}}{Y_2} = (\frac{C_{A0}}{Y_1} + \frac{C_{B0}}{Y_2})(erfc(\frac{z^*}{2\sqrt{D_z \frac{x}{v}}}) + erfc(\frac{2M - z^*}{2\sqrt{D_z \frac{x}{v}}})) \qquad [d]$$

At the point where the plume fringe of electron donor meets the bottom of the aquifer, we have $z^* = M$, $x = L$, where *L* is the length of the plume. So eq [d] can be written as

$$\frac{C_{B0}}{Y_2} = 2(\frac{C_{A0}}{Y_1} + \frac{C_{B0}}{Y_2})erfc(\frac{M}{2\sqrt{D_z \frac{L}{v}}}) \qquad [e]$$

and the plume length equals to

$$L = \frac{M^2 v}{4D_z \left[erfc^{-1}(\frac{1}{2}\frac{Y_1 C_{B0}}{(Y_1 C_{B0} + Y_2 C_{A0})}\right]^2} \qquad [f]$$

Here $erfc^{-1}$ is the inverse of the complimentary error function. The inverse function of complimentary error function can be solved by some mathematical software.

The governing equation and boundary conditions used here are the same as those used in Liedl et al. (2005). However, their solution is implicitly given in an infinite series. Even though in some cases it can be reduced to a simplified equation, it will overestimate the length of the plume.

If the pore diffusion coefficient is negligible in comparison to the mechanical transverse dispersion coefficient, i.e., $D_z \approx \partial_l v$, then we can drop off the velocity from numerate and denominate, which means the velocity has no effect on the length of the steady state plume. So the plume length *L* can be written as:

$$L = \frac{M^2}{4\partial_l \left[erfc^{-1}(\frac{1}{2}\frac{Y_1 C_{B0}}{(Y_1 C_{B0} + Y_2 C_{A0})}\right]^2} \qquad [g]$$

As is shown in [g] the steady state plume length is proportional to the square of the thickness of the aquifer and inversely proportional to the transverse dispersivity. All the reaction terms come to the argument of the inverse complimentary error function.

For an aquifer with a thickness of 2m, $\partial_t = 5$cm. $C_{ED} = 20$mg/l (ammonium) and $C_{EA} = 10$mg/l (oxygen) with a reaction

$$NH_4^+ + 2O_2 \text{---------} NO_3^- + H_2O + 2H^+$$

By neglecting pore diffusion, the above equation yields a steady state plume length of 67 meters.

5. Using oxygen as a tracer to determine the transverse dispersion coefficients

5.1 Objectives

The objectives of this chapter are to verify the analytical solutions of transport of oxygen across the capillary fringe in the laboratory and to apply analytical solutions to determine the transverse hydrodynamic dispersion coefficient using oxygen as a non-reactive and reactive tracer.

5.2 Theoretical background

5.2.1 Non-reactive transport of oxygen across the capillary fringe

In sediments of very uniform grain size and mineralogy, e.g., uniformly sized sand, the water content in the capillary fringe can be an abrupt step function of height above the water table (where P=0) and in such an idealized case the water-content profile would also be independent of sampling location within the studied field (Ronen et al., 1997). Hence, in the given case, the upper boundary of the capillary fringe is very even and the water within the capillary fringe is fully saturated. Above the upper boundary of the capillary fringe the water reaches residual saturation and the gas phase saturation is very high. Due to the high gas saturation the oxygen from the air can easily reach the upper boundary of capillary fringe. In the air film the mass transfer resistance may be assumed negligible because of the relatively low water solubility of oxygen. Thus the concentration at the top of the capillary fringe C_{A0} is directly related to its partial pressure P_A by Henry's law. If we assume the oxygen partial pressure does not change during the experiment then the downward movement of oxygen can be treated as diffusion into semi-infinite domain with a constant concentration boundary condition, as is shown in Figure 5.1.

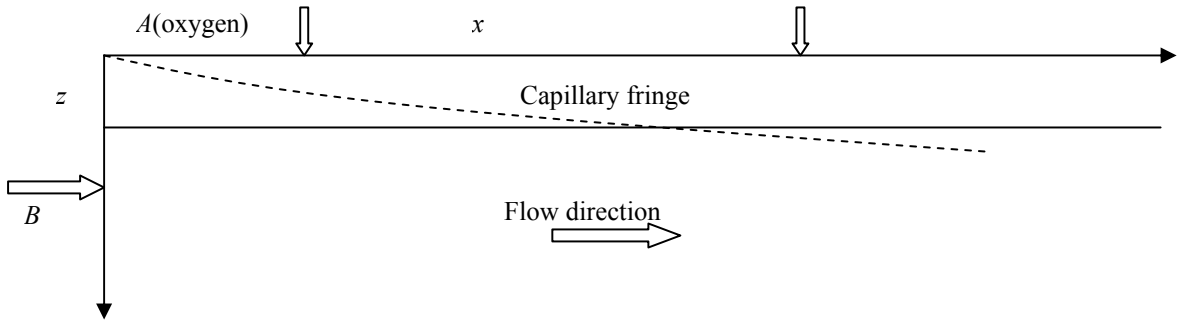

Figure 5.1 Diffusion of oxygen through the fully saturated capillary fringe into groundwater. (the dotted line denotes the oxygen front and the horizontal solid line denotes the water table).

Diffusion into a semi-infinite domain according to Fick's second law in 1D is given by

$$\frac{\partial C}{\partial t} = D_z \frac{\partial^2 C}{\partial z^2} \qquad [5.1]$$

By replacing t with x/v the above 1D transient state case can be applied to 2D steady state case

$$v\frac{\partial C}{\partial x} = D_z \frac{\partial^2 C}{\partial z^2} \qquad [5.2]$$

C [mg/l] is dissolved oxygen concentration, v [m/s] is the pore velocity and D_z [m^2s^{-1}] is the hydrodynamic transversal dispersion coefficient, which is commonly defined as:

$$D_z = D_{pore} + \alpha_t v \qquad [5.3]$$

D_{pore} denotes the pore diffusion coefficient which according to Boving and Grathwohl (2001) is approximately:

$$D_{pore} \cong n\ D_{aq} \qquad [5.4]$$

In this case eq [2] is subjected to the following conditions:

$$x = 0,\ C = C_{bg} \qquad [5.5]$$

$$z = 0,\ C = C_0 \qquad [5.6]$$

$$z = +\infty,\ C = C_{bg} \qquad [5.7]$$

C_{bg} is the background concentration of oxygen and C_0 is the concentration at the air water interface.

The concentration profile can be obtained by solving equation [5.2] through the method of 'combination of variables' (Boltzmann, 1894)

$$C = C_{bg} - (C_{bg} - C_0)\,erfc\left(\frac{z}{2\sqrt{D_z \frac{x}{v}}}\right) \qquad [5.8]$$

The above equation can be normalized by moving C_{bg} to the left side and dividing both sides with $(C_0 - C_{bg})$, which is

$$C_{norm} = \frac{C - C_{bg}}{C_0 - C_{bg}} = erfc\left(\frac{z}{2\sqrt{D_z \frac{x}{v}}}\right) \qquad [5.9]$$

In this solution the only unknown parameter is the transverse hydrodynamic dispersion coefficient D_z, which can be obtained by fitting the equation to the experimental data.

5.2.2 Reactive transport of oxygen across the capillary fringe

For the reactive case, we assume an instantaneous reaction between oxygen and the electron donor. Thus this process becomes analogous to diffusion into a semi-infinite domain with an instantaneous reaction. Similar scenarios have been studied by Dankwerts (1970) for the absorption of gas into quiescent liquids. The solution for the diffusive gas is (modified after Dankwerts, 1970)

$$C/C_{A0} = \frac{erfc(z/2\sqrt{D_{tA}t}) - erfc(\beta\sqrt{D_{tA}})}{erf(\beta/\sqrt{D_{tA}})} \qquad [5.10]$$

where β may be solved by the iterative solution of:

$$e^{\beta^2/D_B} erfc(\beta/\sqrt{D_{tB}}) = \frac{Y_1 C_{B0}}{Y_2 C_{A0}} \sqrt{(\frac{D_{tB}}{D_{tA}})} e^{\beta^2/D_{tA}} erf(\beta/\sqrt{D_{tA}}) \quad [5.11]$$

Y_1 and Y_2 are the stoichiometries of oxygen and the electron donor; C_{A0} is the concentration of oxygen at the upper limit of the capillary fringe. C_{B0} is the initial concentration of electron donor that is supplied with the system. D_{tA} and D_{tB} are hydrodynamic dispersion coefficients of oxygen and the electron donor.

If we assume $D_{tA} = D_{tB} = D_z$ then the above equation can be simplified (see chapter 4) to the following equation:

$$C_{norm} = \frac{C_A}{C_{A0}} = (1 + \frac{C_{B0}}{C_{A0}} \frac{Y_1}{Y_2}) erfc(\frac{z}{2\sqrt{D_z \frac{x}{v}}}) - \frac{Y_1}{Y_2} \frac{C_{B0}}{C_{A0}} \quad [5.12]$$

where C_{norm} is the normalized concentration of oxygen.

5.2.3 Instantaneous reaction

All reactions proceed at a finite rate, and the concept of an 'instantaneous' reaction is an idealization. Reactions of finite speed can, under certain circumstances, be treated as if they were instantaneous; this would be to assume that under these circumstances the rate of reaction is controlled entirely by the diffusion of the reactants to the site of the reaction (Dankwerts, 1970).

The reaction between dissolved oxygen with sodium sulfite has been studied for flue gas desulphurization (FGD) a long time. A lot of experiments have been carried out to investigate the influence of sulfite concentration, oxygen partial pressure, catalyst concentration, pH on the reaction order, and rate. The normally slow reaction is specifically accelerated by certain metal ions such as Co^{2+}, Cu^{2+}, Fe^{2+}, Mn^{2+}, etc. (Linek and Vacek, 1981). Among them $Co^{2+}$and $Cu^{2+}$are commonly used. However, cobalt catalysts give about twelve time faster rate than copper catalysts. The oxidation

of sulfite is slow at low pH but proceeds rapidly in basic solution in the presence of cobalt ion as catalyst (Kessick, 1976). Linek and Vacek (1981) found that Co^{2+} will catalyze the reaction at concentration of 10^{-7}-10^{-4} mol/L. The strong catalytic effect of the catalysts in use practically make the reaction fast enough for all absorbed oxygen to react in the bulk of the liquid near the interface, which prevents the coexistence of oxygen and sulfite. Wainwright and Johnson (1980) examined the oxidation of sulfite added as a sodium sulfite solution to soils of different moisture content. They found that the oxidation rates decreased with increasing moisture content, which indicated that available oxygen is the limiting factor. The liquid-phase reaction can be described by the overall stoichiometric equation:

$$O_2 + 2SO_3^{2-} \rightarrow 2SO_4^{2-} \qquad [5.13]$$

5.3 Experimental setup

The experimental setup is quite similar to Olsson (2007) and Eberhardt (2000), i.e., a tank system. The quasi two-dimensional tank has a dimension of 80cm*10cm*1cm. Both outlet and inlet were equipped with 11 ports. The interval between two ports was 8mm. These ports were connected via stainless steel capillaries (0.8mm) and viton tubes (0.6 mm in diameter) to two peristaltic pumps, which were operated at the same pumping rate for the pumping in and the pumping out of the solution to and from the tank, i. e., the flow boundaries at the left and right were constant flux boundaries. These boundary conditions are more complicated than the constant head boundary conditions in that the hydraulic head inside the tank depends on the pumping rate. The higher the pumping rate, the higher the hydraulic head at the inlet and the lower the hydraulic head at the outlet. The parabolic head distribution along the flow direction depends also on the hydraulic conductivity of the system, while for the constant head boundary condition the head distribution inside the tank only depends on the heads at the inlet and outlet (see Appendix 1). Additionally, the initial water table is important for the constant flux boundary conditions because it determines the final water table after the flow reaches steady state.

The gradient established inside the tank causes a deviation of the experiment setup from the conceptual model, which assumes a perfect horizontal water surface. This is especially the case when flow velocities are high, because the tilting of the water table will become much steeper. If the velocity is high enough, for example, $v \geq k\frac{H}{L}$, where k is the hydraulic conductivity of the porous media and H and L are the height and the Length of the tank, some of the water at the inlet will have to flow to the outside of the tank. To get rid of the effect of the titling water table, a low flow velocity or a porous media with higher hydraulic conductivity should be used.

The walls of the tank were made of transparent sheet glasse and had a thickness of 4mm (thin enough for the light to transmit). The tank was filled with artificial glass beads (quartz) with diameters ranging from 1.0 to 1.5 mm. Since uniform glass beads were used, special packing procedures were not deemed necessary in order to achieve homogeneous samples, with the exception of light tapping on the walls which proved to be an efficient means of compacting the sand in the boundary zones (Pantazidou and Sitar, 1993). To make sure the system is already at steady state, the measurements were taken after at least two pore volumes.

The glass beads were put into the tank under saturated conditions except for a few centimeters at the top. Slightly stirring with a glass stick while filling was necessary to get rid of entrapped air bubbles. The top few centimetres were kept unsaturated and by capillary force a capillary fringe of about 2.2 centimeters for the 1-1.5mm diameter glass beads was formed and above it was the unsaturated zone. To reduce evaporation the tank was covered with a plastic lid, which still allowed gas exchange.

5.3.1 Non-reactive experiment

For the non-reactive case, the deoxygenated water (deionized water after being purged of oxygen with nitrogen gas) was pumped into the tank system through the inlet ports via viton tubing (Ismatec) from the Tedlar bag. Due to the diffusion of a small amount of oxygen through the tubing, the deoxygenated water pumped into the tank contained a small amount of oxygen, which was treated as the background oxygen.

5.3.2 Reactive experiment

For the reactive case, instead of deoxygenated water, sodium sulfite solution was pumped into the tank. As can be seen in equations [10] and [11], the oxygen concentration and also penetration depth strongly depend on the injected concentration of electron donor sulfite. Since the penetration depth ranges usually from several mm to several cm, the concentration of sulfite should be kept small to achieve a higher penetration depth and, therefore, more data. The initial concentration of sulfite was measured with ion chromatography (Dionex). Because sulfite is easily oxidizable, during the sampling and measuring with IC it had to be stabilized as soon as it went to the sampling vials. Sulfite can be stabilized by formaldehyde-sodium hydroxide solution. The stabilizing solution was prepared by adding 1ml formaldehyde (37%) and 1ml sodium hydroxide (0.1mol/l) to 1 litre deoxygenated water. As is described in the non-reactive case, due to the diffusion of small amount of oxygen through the tubing during the transport of sodium sulfite to the tank, some of the sulfite had already been oxidized before it entered the tank. The concentration of sulfite that was pumped into the tank was therefore a little bit lower than concentration in the Tedlar bag. This concentration is the initial concentration C_{B0}.

In addition to the sulfite solution, cobalt chloride ($CoCl_2$) with a concentration of 2×10^{-4} mol/l was also added into the Tedlar bag to catalyze the reaction. The reaction proceeds more rapidly in basic solution. However, if the pH is too high, the cobalt ion will react with OH^- to form the green colored $Co(OH)_2$ precipitate which will reduce the catalyzing effect and also cause a reduction of the hydraulic conductivity of the glass beads.

5.3.3 Measurement of oxygen

For the measurement of oxygen concentration, a non-invasive measurement technique was used (Fibox 3, Presens, Germany). The principle of the sensor operation is based on the quenching of luminescence caused by collision between molecular oxygen and luminescence dye molecules in the excited state. A relation exists between the oxygen concentration in the sample and the luminescence intensity as well as the luminescence lifetime which is described in the Stern-Volmer equation (Presens). For

the non-invasive measurement of oxygen we first glued an oxygen sensitive foil with a width of 5mm (wide enough for the light spot produced by the LED to lie within) and a length of 5cm (long enough in comparison with the penetration depth of oxygen from the top of the tank) to the inner wall of the tank (see figure 2). A raster about the same size of the oxygen sensitive foil was attached on the outside wall of the tank to fix an optical fibre. The optical fibre with a diameter of 2mm was used to transmit the light between a LED and the foil. A series of holes with a diameter of 2mm in the vertical direction were drilled onto the raster to keep the optical fibre perpendicular to the outside wall of the tank (in order to eliminate light refraction) and also to help the fibre pinpoint the exact location of measurement.

To avoid the tank boundary effects at the inlet and outlet part, the oxygen sensitive foil was located 60 cm away from the inlet on the inner wall of the tank as is shown in Figure 2.

Figure 5.2 Tank used in the experiment (the red tape is the oxygen sensitive foil which is glued on the inner wall of the tank)

5.4 Result from the non-reactive case

In order to investigate the transverse vertical dispersion coefficients under different velocities for the same porous media, we ran the experiment under three different velocities for the non-reactive and reactive cases. These were done by changing the pumping rate and switching the bulk solution from deoxygenated water to the sodium sulfite solution in the Tedlar bag. Vertical oxygen concentration profiles were obtained non-invasively for each case.

The oxygen concentration obtained through the non-invasive measurement for the non-reactive case is shown in Figure 5.3. The background concentration of oxygen

here was about 2 mg/l. This did not affect the results because it was kept constant during the experiment. The pink hollow squares represent the measured oxygen concentrations and solid blue line represents the fitted concentration using equation [2]. As can be seen from this figure, the measurement fits the model prediction very well. The unsaturated part offers almost no resistance to the diffusion of oxygen and therefore there is a very small gradient developing there. As soon as oxygen approaches the upper boundary of the capillary fringe the gradient develops rapidly, which means the limiting part of the mass transfer lies in the water saturated part of the capillary fringe. Based on the gradients near the upper boundary of the capillary fringe, we obtained an effective gaseous oxygen diffusion coefficient of 2.0e-7 m^2/s for the unsaturated part. This value was further used to calculate the average water content according to Millington correction: an average value (6mm from the upper boundary of CF) of 62% could also be obtained. This water saturation is reasonable if we compare these results to the modelling results from chapter 3 which show that the oxygen gradient only develops rapidly after it reaches 85% water saturation.

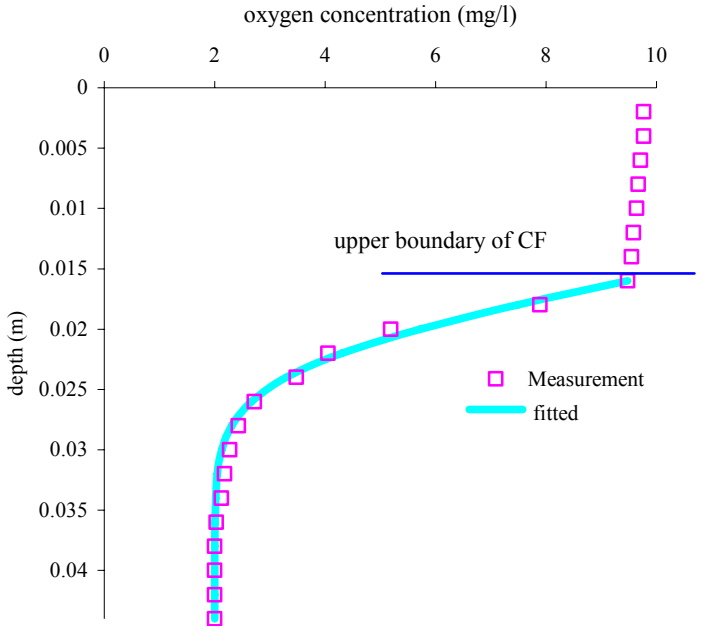

Figure 5.3 Vertical oxygen concentration profile.

Figure 5.4 shows the normalized concentration profiles of oxygen at flow velocities 3.95 m/day, 7.33 m/day and 16.4 m/day.

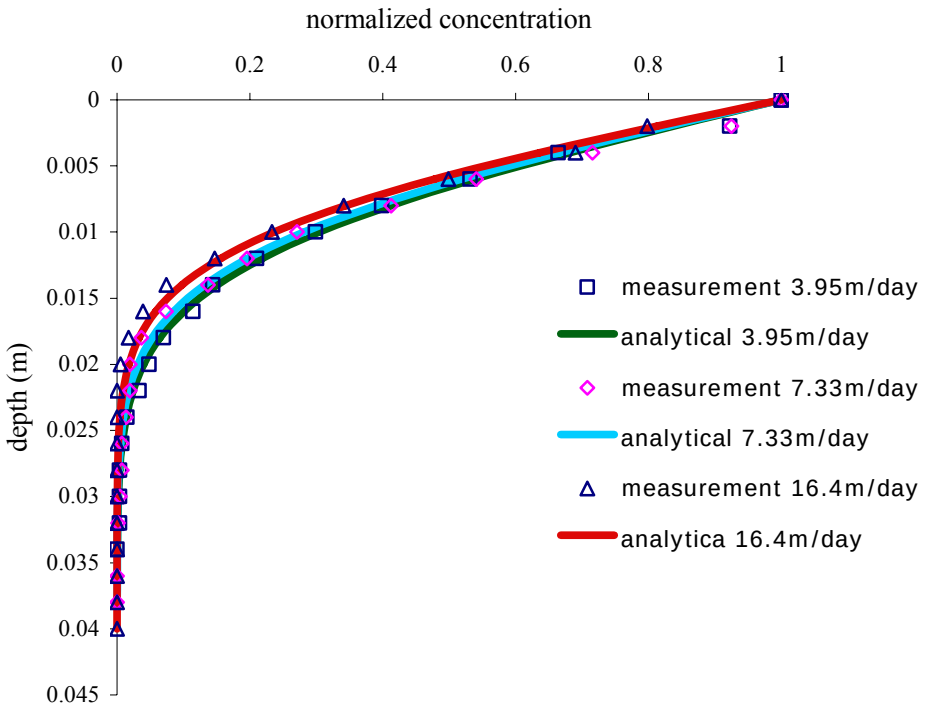

Figure 5.4 Normalized oxygen concentrations under three different velocities

All the three measurements in Figure 5.4 agree well with the analytical solution, which further proves the conceptual model of diffusion into semi-infinite domain. For the higher flow velocities, slightly smaller oxygen penetration depths were measured. But this effect of the horizontal flow velocities on the vertical oxygen concentration profiles is not significant and at moderate velocities 3.95 and 7.33 m/day the measurements are almost identical, which means pore diffusion is not important and this process is dominated by mechanical dispersion. The parameters used in the curve fittings are listed in Table 5.1.

Table 5.1 Fitted hydrodynamic dispersion coefficients under three different velocities

C_{bg}(mg/l)	C_0 (mg/l)	v(m/day)	D_z(m^2/s)
6,67	9,38	3,95	3,62e-9
2,22	9,19	7,33	6,11e-9
1,79	9,21	16,4	1,33e-8

As is mentioned in the previous chapter, the high background oxygen concentration at slow flow velocity in Table 5.1 was due to the long travelling time for the solution from the Tedlar bag to the tank, which caused more oxygen to diffuse through the tubings into the solution. From the fitted D_z values we can also see that the

contribution of pore diffusion ($2e^{-9}$ * 0.35 =$7e^{-10}$ m^2/s) to the overall hydrodynamic dispersion coefficient at flow velocity 3.95 m/day is about 20 percent. With the increase of velocity it becomes more and more insignificant; at velocities of 7.33 and 16.4 m/day it is only 10 and 5 percent, respectively. There is an almost linear increase of transverse hydrodynamic dispersion coefficient with the flow velocity.

5.5 Results from reactive case

5.5.1 Effect of cobalt chloride

In order to find out whether the reaction rate is limiting this process or not we measured and compared the oxygen concentration profile for the same porous media under the same velocity (7.33 m/day) but with two different solutions. Both of these solutions have the same sulfite concentration of 65 mg/l but one with catalyst cobalt (2×10^{-4} mol/l) and one without. As was shown in the previous chapter, the cobalt can catalyze the normally slow reaction. If oxygen transfer is limited by the reaction rate, then the concentration profile with faster reaction should have a sharper gradient. Figure 5.5 shows the oxygen profiles obtained from these two solutions.

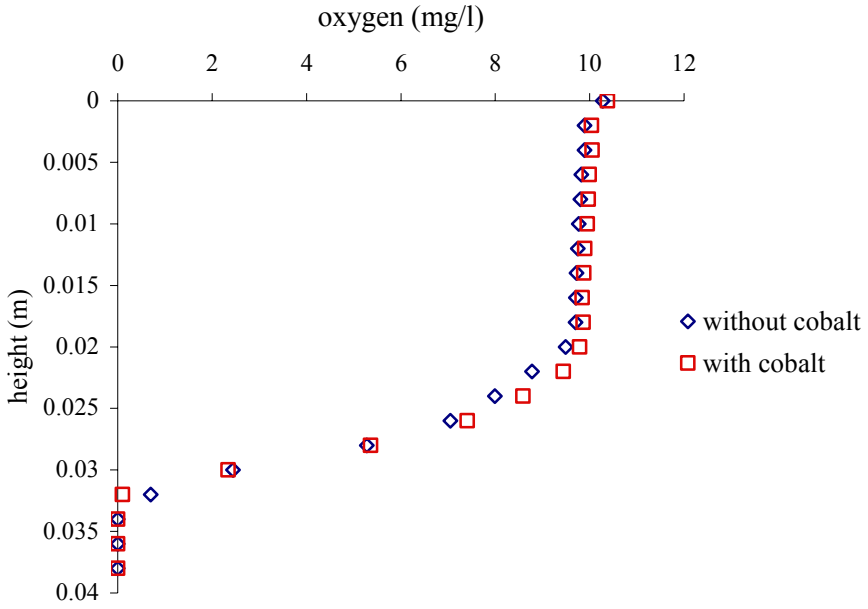

Figure 5.5 Reactive oxygen concentration profiles for the case with and without catalyst

The results did not show a significant change of oxygen profile, which means the reaction rate in this case does not limit the mass transfer process.

5.5.2 Vertical oxygen profiles under three velocities

For the reactive case, the vertical oxygen concentration profiles under different velocities are shown in Figure 5.6. The parameters used in the fitting are listed in Table 5.2. The same transverse hydrodynamic dispersion coefficients obtained from the non reactive case were used to fit equation [5.11]. Again equation [5.11] is in good agreement with the experimental data. In comparison to the non-reactive case the reactive case has a steeper gradient (Figure 5.7) and the vertical concentration profiles are almost linear.

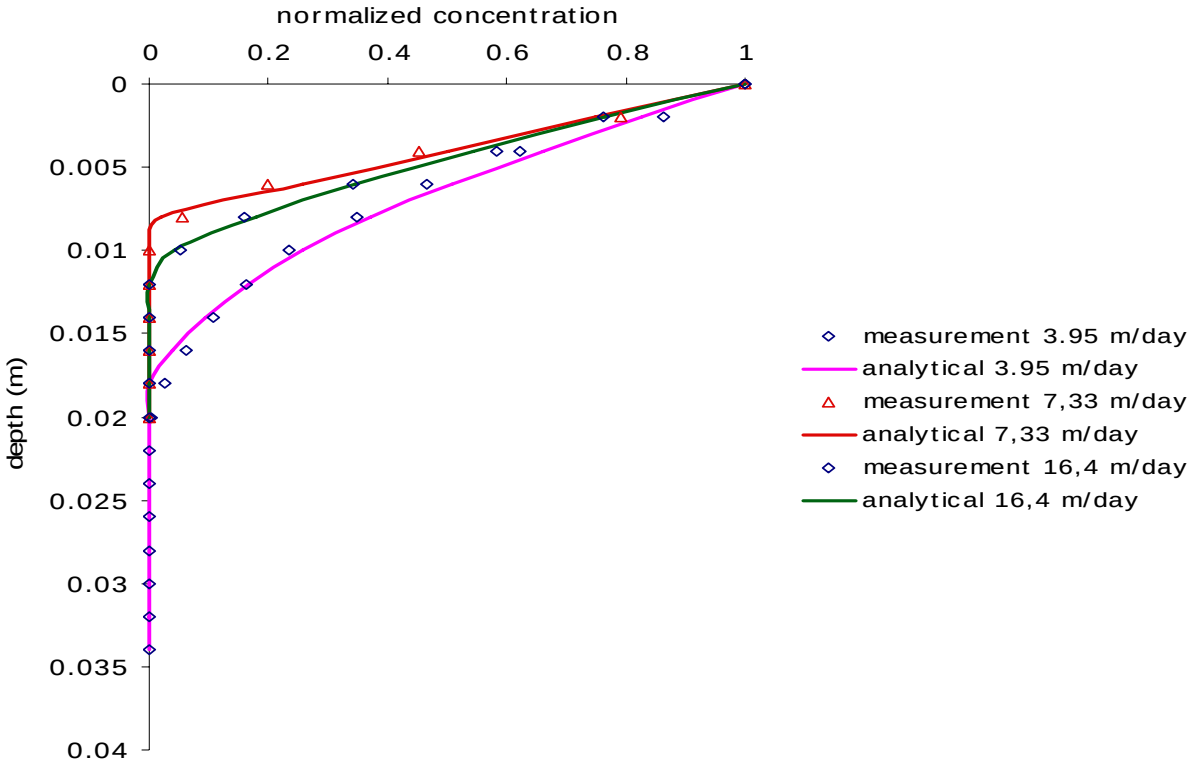

Figure 5.6 Vertical concentration profiles under different velocities (reactive case)

Table 5.2 Parameters used in the fitting for the reactive case

C_{A0} (mg/l)	C_{B0} (mg/l)	v(m/day)	D (m^2/s)
3,25	9,38	3,95	3,62e-9
25,90	9,19	7,33	6,11e-9
11,60	9,21	16,4	1,33e-8

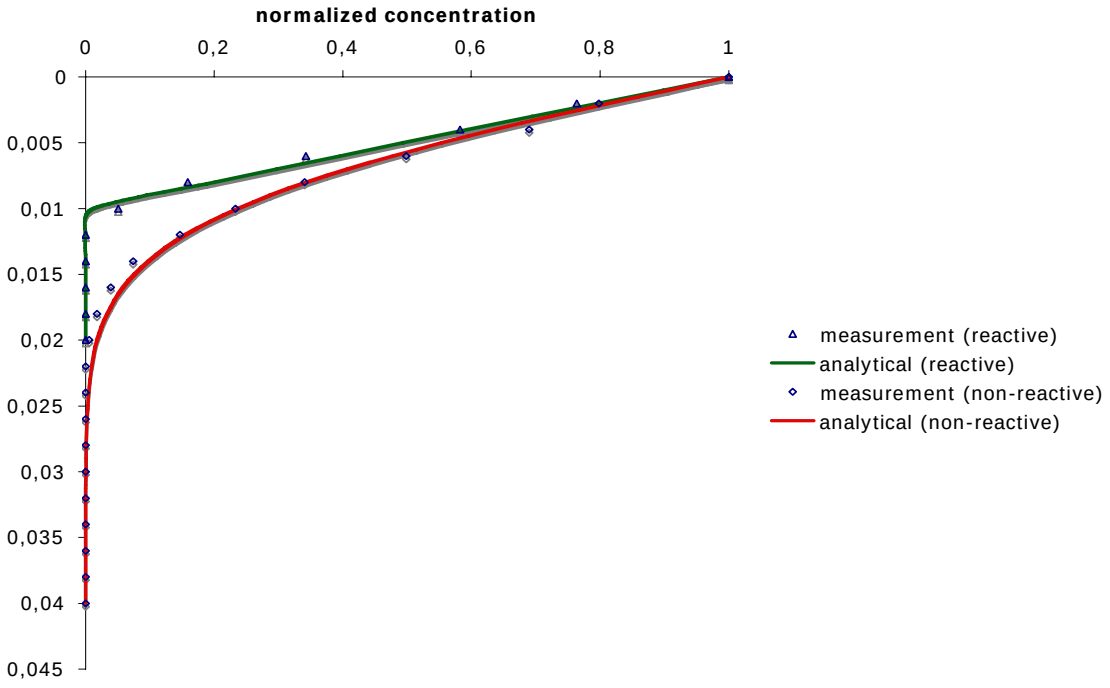

Figure 5.7 Comparison of the concentration profiles under the same velocity for the reactive and non-reactive case for flow velocity 16.4m/day.

5.5.3 Tank boundary effect

To investigate the boundary effects at the inlet we glued another oxygen sensitive foil at a location 10 cm away from the inlet (see Figure 5.8).

Figure 5.8 Additional oxygen sensitive foil near the inlet to investigate the boundary effect

The measured and fitted oxygen concentration profiles from both foils and for the non reactive and reactive are shown in the following Figure 5.9 and 5.10. The hydrodynamic dispersion coefficients obtained at x=10 cm and 60 cm are 7.2e-9 m^2/s and 4.5e-9 m^2/s respectively. The higher hydrodynamic dispersion coefficient near the

inlet indicates that the flow condition near the boundary is more complex than in the middle of the tank. This can be further verified by the numerical simulation result of the velocity vectors in the system (see Appendix 2).

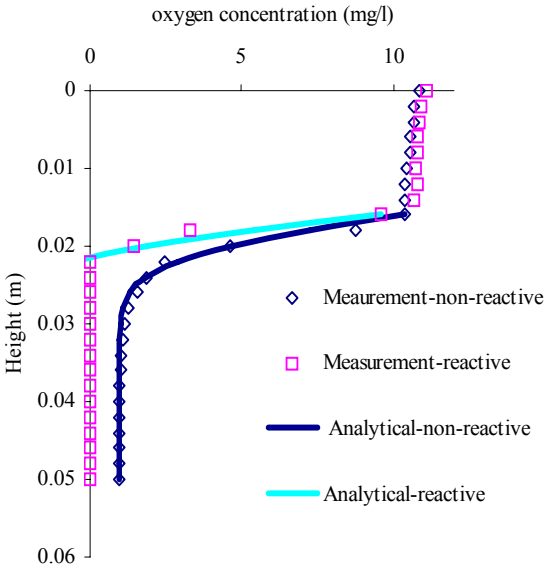

Figure 5.9 Oxygen concentration profile at x= 10 cm

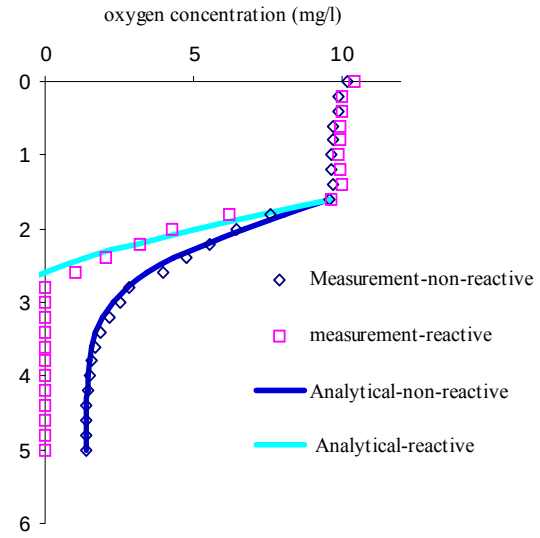

Figure 5.10 Oxygen concentration at x= 60 cm.

5.6 Discussion

The reaction rate of sulfite with oxygen is usually very slow. Even though we added cobalt chloride and adjusted the pH in these experiments to speed up this reaction, it may be still not fast enough so that sulfite and oxygen can coexist. This could explain why in some cases the oxygen could go deeper than predicted by the analytical model. In addition, whether the reaction was fast enough to be called 'instantaneous' not only depends on the reaction rate but also the residence time of the reactants in the system, i.e., the transport timescale has to be much bigger than one for a reaction to be called instantaneous (a high Damköhler number). Due to the complex dependence of the reaction rate and order on the reactants concentrations, catalyst concentration, and also pH, we did not measure the reaction rate. Therefore we didn't quantify the Damköhler numbers in our experiment. But our results show that in our experiments, the reaction was already fast enough to be called 'instantaneous'.

The assumption of same hydrodynamic dispersion coefficients for all the reaction compounds can be validated as long as the flow velocity is not too slow. Even though the diffusion coefficient of aqueous oxygen is twice as great as those of sulfite and sulfate, our experiments were always dominated by mechanical dispersion.

The capillary fringe in the experiment likely is not 100% saturated. But the effect of less than 100% saturation on D_z is the same for the non-reactive and the reactive case, so it did not affect our results.

5.7 Conclusions

1. The models which assume that the oxygen transfer across the capillary fringe can be treated as diffusion into semi-infinite domain with and without instantaneous reaction are validated by the experiments.

2. Oxygen can be used as a non-reactive and reactive tracer to determine the hydrodynamic dispersion coefficients. This is advantageous because non invasive measurement of oxygen, in contrast to some other methods, has a high resolution and is relatively easy to handle.

3. The oxygen gradient develops in the saturated part of the capillary fringe; therefore, mechanical dispersion dominates the transfer process and transverse dispersion is the limiting factor.

4. The hydrodynamic dispersion coefficients obtained from non-reactive case and reactive cases agree with each other.

Appendix 1: Hydraulic head under constant head and constant flux boundary conditions

For the constant head boundary conditions in an unconfined porous medium, i.e. the hydraulic heads h_1 and h_2 at inlet and outlet are given, the hydraulic head in the flow direction can be easily derived through Darcy's law and written explicitly as

$$h(x) = \sqrt{h_1^2 - \frac{(h_1 + h_2)(h_1 - h_2)}{L}x} \qquad [1]$$

L is the length of the tank. Equation [1] shows that the head within the tank only depends on the hydraulic heads at the inlet and outlet.

For the constant flux boundary, if we know the flux Q (pumping rate) and initial water table h_{inital} before pumping, the hydraulic head can be written according Darcy's law as

$$h(x) = \sqrt{h_1^2 - \frac{2Q}{k}x} \qquad [2]$$

where h_1 is the still unknown water head at the inlet. The water head at the inlet can be obtained based on the water balance inside the tank, because the total volume of water within the tank should always equal the initial volume of water before pumping, which is

$$\int_0^L \sqrt{h_1^2 - \frac{2Q}{k}x}\,dx = h_{initial}L \qquad [3]$$

Therefore h_1 can be written implicitly as

$$h_1^3 - (h_1^2 - \frac{2Q}{K}L)^{\frac{3}{2}} = \frac{3h_{initial}QL}{K} \qquad [4]$$

This indicates that for the constant flux boundary condition the head at the inlet h_1 depends on the pumping rate and the hydraulic conductivity of the porous media.

Appendix 2: Boundary effects at the inlet and outlet of the tank

Figure 5.a shows the velocity vectors under constant flux boundary conditions. At inlet and outlet the flow vectors have larger vertical components than in the middle part of the tank, which indicates that there is more mixing at the inlet and outlet.

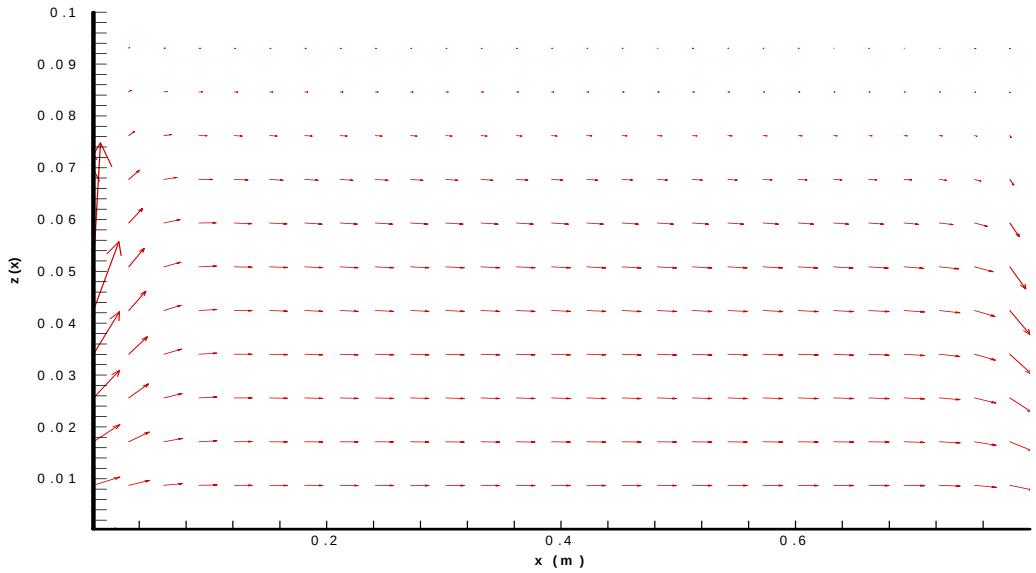

Figure 5.a Velocity vectors inside the tank.

References

Bertelsen, F., Gissel-Nielsen, Gunnar., 1988. Oxidation of sulphite originating from flue gas desulphurization waste in soil. Environmental Geochemistry and Health, 10 (1), 26-30.

Boltzmann, L., 1894. Annalen der Physik und Chemie, 53, 959

Boving, T., Grathwohl, P., 2001. Matrix diffusion coefficients in sandstones and limestones: Relationship to permeability and porosity. J. Cont. Hydrol. 53 (1-2), 85-100.

Danckwerts, P.V., 1970. Gas–Liquid Reactions. McGraw-Hill, New York.

Johnson, R.L., Pankow, J.F., 1992. Dissolution of dense chlorinated solvents into groundwater. 2. Source functions for pools of solvent. Environ. Sci. Technol. 26, 896-901.

Kessick, M., 1976. The calibration of closed-end manometric biochemical oxygen demand respirometers. Biotechnology and Bioengineering, vol (18), 595-598.

Linek, V., Vacek, V., 1981. Chemical engineering use of catalyzed sulfite oxidation kinetics for the determination of mass transfer characteristics of gas-liquid contactors. Chemical Engineering science 36, 1747-1768.

Ronen,D., Scher,H., Blunt,M.J., 1997. On the Structure and Transport Properties in the Capillary Fringe of Phreatic Aquifers, Transport in Porous Media. Vol: 28, Pages: 159 – 180.

Olsson, Å., Grathwohl, P., 2007. Transverse dispersion of non-reactive tracers in homogeneous porous media: a new nonlinear relationship to predict dispersivity. J. Cont. Hydrol. 92, 149-161.

Pantazidou, M., Sitar, N., 1993. Emplacement of nonaqueous liquids in the vadose zone. Water Resour. Res. 29, 705 – 722.

Wainwright, M., Johnson, J., 1980. Determination of sulphite in mineral soil. Plant and Soil 54, 299-305.

6. Summary

The numerical modeling results of reactive transfer of oxygen across the capillary fringe show that due to the low horizontal velocity in the unsaturated zone there is an accumulation of reaction product there. The maximum concentration of reaction product depends only on the concentration of electron donor, not electron acceptor. The oxygen gradient starts to develop when the water saturation reaches about 85%.

The numerical modeling results are further verified by the analytical solutions. In addition, the analytical solutions also provide the spatial distributions of the reactants and reaction product and also the closed form equation to describe the length of electron donor plume.

The analytical models which assume the mass transfer of oxygen across the capillary fringe to be diffusion into semi-infinite domain with and without reaction are also proved by lab experiments. The experimental results show that no or little oxygen gradient develops in the unsaturated zone. The oxygen gradient starts to develop rapidly as soon as it reaches highly saturated capillary fringe. Velocity doesn't have a significant effect on the oxygen concentration profile, which indicates this mass transfer process is dominated by mechanical dispersion. Compared to the non-reactive case, the reactive case has a sharper oxygen gradient, which is almost linear.

The hydrodynamic dispersion coefficient can be obtained by fitting the analytical solutions to the high resolution data. This provides a new method using oxygen as a non-reactive and reactive tracer to determine the hydrodynamic dispersion coefficient. In comparison to some other traditional sampling at ports methods, it is easy to handle and has a high resolution. The hydrodynamic dispersion coefficients obtained from reactive and non-reactive cases are the same for the same porous media under the same velocity.